

SCIENCE OF TSUNAMI HAZARDS

The International Journal of The Tsunami Society
Volume 27 Number 1 Published Electronically 2008

TSUNAMI HAZARD ASSESSMENT IN THE NORTHERN AEGEAN SEA 1

Barbara Theilen-Willige,

Berlin University of Technology (TU Berlin), Institute of Applied Geosciences, Department of Hydrogeology and Bureau of Applied Geoscientific Remote Sensing (BAGF), Stockach, Germany.

**LARGE BOULDERS ALONG THE RABAT COAST (MOROCCO); POSSIBLE
EMPLACEMENT BY THE NOVEMBER, 1st, 1755 A.D. TSUNAMI** 17

Nadia Mhammdi, Fida Medina,

Université Mohammed V-Agdal, Institut Scientifique, Département des Sciences de la Terre, Rabat, Morocco.

Dieter Kelletat,

Universität Köln, Institut für Geographie, Koeln, Germany.

M'Fedal Ahmamou, Lamiaa Aloussi, *Université Mohammed V-Agdal, Faculté des Sciences, Département des Sciences de la Terre, Rabat, Morocco.*

TSUNAMIS OF THE ARABIAN PENINSULA A GUIDE OF HISTORIC EVENTS 31

Benjamin R. Jordan,

Department of Geology Brigham Young University Rexburg, Idaho, U.S.A

**A STUDY OF GROUNDWATER QUALITY IN TSUNAMI AFFECTED AREAS OF SIRKAZHI
TALUK, NAGAPATTINAM DISTRICT, TAMILNADU, INDIA** 47

N. Ravisankar and S. Poongothai,

Dept. of Civil Engineering, Annamalai Univ., Annamalainagar, India

THE TSUNAMI SOCIETY
P. O. Box 2117, Ewa Beach, HI 96706-0117, USA,
[WWW.TSUNAMISOCIETY.ORG](http://www.tsunamisociety.org)

OBJECTIVE: The Tsunami Society publishes this journal to increase and disseminate knowledge about tsunamis and their hazards.

DISCLAIMER: Although these articles have been technically reviewed by peers, The Tsunami Society is not responsible for the veracity of any statement, opinion or consequences.

EDITORIAL STAFF

Dr. George Pararas-Carayannis, Editor
1741 Ala Moana Blvd. No 70, Honolulu, Hawaii 96815, USA

EDITORIAL BOARD

Dr. Charles MADER, Mader Consulting Co., Colorado, New Mexico, Hawaii, USA
Dr. Hermann FRITZ, Georgia Institute of Technology, USA
Prof. George CURTIS, University of Hawaii -Hilo, USA Dr. Tad S. MURTY, Ottawa, Canada
Dr. Zygmunt KOWALIK, University of Alaska, USA
Dr. Galen GISLER, Norway
Prof. Kam Tim CHAU, Hong Kong Polytechnic University, Hong Kong
Dr. Jochen BUNDSCHUH, (ICE) Costa Rica, Royal Institute of Technology, Stockholm, Sweden
Dr. Yuri SHOKIN, Novosibirsk, Russian Federation

TSUNAMI SOCIETY OFFICERS

Dr. George Pararas-Carayannis, President; Dr. Tad Murty, Vice President; Dr. Gerard Fryer, Secretary; Dr. Vindell Hsu, Treasurer.

Submit manuscripts of articles, notes or letters to the Editor. If an article is accepted for publication the author(s) must submit a scan ready manuscript, a Doc, TeX or a PDF file in the journal format. Issues of the journal are published electronically in PDF format. Recent journal issues are available at:
<http://www.TsunamiSociety.org>
<http://www.sthjourn.org>

Tsunami Society members will be advised by e-mail when a new issue is available. There are no page charges for one paper per calendar year for authors who are members of the Tsunami Society. Permission to use figures, tables and brief excerpts from this journal in scientific and educational works is hereby granted provided that the source is acknowledged.

Issues of the journal from 1982 thru 2005 are available in PDF format at
<http://epubs.lanl.gov/tsunami/> and on a CD-ROM from the Society to Tsunami Society members. ISSN 8755-6839 <http://www.sthjourn.org>

TSUNAMI HAZARD ASSESSMENT IN THE NORTHERN AEGEAN SEA

Barbara Theilen-Willige

Berlin University of Technology (TU Berlin),
Institute of Applied Geosciences, Department of Hydrogeology and
Bureau of Applied Geoscientific Remote Sensing (BAGF),

Birkenweg 2, D-78333 Stockach, Germany,

e-mail: Barbara.Theilen-Willige@t-online.de

ABSTRACT

Emergency planning for the assessment of tsunami hazard inundation and of secondary effects of erosion and landslides, requires mapping that can help identify coastal areas that are potentially vulnerable. The present study reviews tsunami susceptibility mapping for coastal areas of Turkey and Greece in the Aegean Sea. Potential tsunami vulnerable locations were identified from LANDSAT ETM imageries, Shuttle Radar Topography Mission (SRTM, 2000) data and QuickBird imageries and from a GIS integrated spatial database. LANDSAT ETM and Digital Elevation Model (DEM) data derived by the SRTM-Mission were investigated to help detect traces of past flooding events. LANDSAT ETM imageries, merged with digitally processed and enhanced SRTM data, clearly indicate the areas that may be prone to flooding if catastrophic tsunami events or storm surges occur.

Key Words: Aegean Sea, tsunami hazard, remote sensing, GIS, morphometric terrain analysis

1. INTRODUCTION

The present study concentrates on tsunami susceptibility mapping for coastal areas in the Aegean Sea where the geomorphologic and lithologic characteristics are similar to areas struck by recent catastrophic tsunamis in the Island of Sumatra, where historic records of floods and tsunami events are available and reliable for purposes of comparison. Disaster emergency planning requires development of maps that delineate the hazard for coastal areas that are susceptible to future tsunami impact. There is a high potential for the generation of large tsunamis around the Aegean Sea, as well as for destructive local events in near-shore zones. The historic record shows that parts of both the Turkish and Greek coastlines were struck by destructive tsunamis (Yalciner et al., 2001, 2004). Most of the historic tsunamis have occurred along well known geologic fault zones and volcanoes. However, there are numerous other areas that can generate destructive tsunamis in the Mediterranean region in the future. Potential tsunamigenic source areas should include the normal fault zones and the subduction zone in the Tyrrhenian sea (Yolsal and Taymaz, 2003; 2004; 2005).

The impact and spatial destructiveness of a potential tsunami will depend on such factors as: a) Width of the continental shelf; b) Near-shore bathymetry (Wijetunge, 2006); c) Energy focusing effects; d) Coastal topography; e) Tsunami terminal velocity and runup height; f) Type of land use in the affected coast - including density of vegetation and buildings.

However, detailed studies are necessary to understand and determine the way by which the above factors could influence the spatial variations in the extent of inland flooding, maximum tsunami runup heights and the degree of damage along the affected coastline. Such information would help determine the degree of vulnerability of the coastal communities to future tsunami events, as well as to storm surges. Although storm surges are not potentially as destructive as major tsunamis, they occur more frequently. Therefore, for effective emergency planning and tsunami preparedness both near and far field effects of potential future tsunamis must be considered. Also, it is important to prepare maps that illustrate the extent by which a coastal area could be inundated by tsunamis and storm surges and to identify potentially vulnerable areas.

2. APPROACH

The present study explores a strategy adopted to generate maps that illustrate areas vulnerable to tsunamis and secondarily-induced effects such as landslides. The methodology is based on the support provided by a standardized, spatial GIS database for the delineation of potential hazard sites. To establish a cost effective method and a quick determination of factors that influence damage intensity in tsunami prone areas, one must analyze the preparatory or causal controlling factors using remote sensing and GIS methodology. For a better understanding of the complex processes and their interactions during tsunami inundations, emphasis is put on a spatially accurate, GIS integrated representation of those influencing parameters and determining factors - provided that such data is available. For example, such parameters as height, slope degree and/or curvature of slopes, can be derived from digital elevation models (DEM). On a regional scale, the areas of potential tsunami risk in the Aegean Sea are determined by an integration of remote sensing data, geologic, seismotectonic and topographic data, and reports of historical tsunamis.

LANDSAT ETM and DEM data were used as layers for generating a Tsunami Hazard GIS and combined with various geodata. For the purpose of the present study the following digital elevation data were evaluated: Shuttle Radar Topography Mission -SRTM, 90 m resolution) data

provided by the University of Maryland, Global Land Cover Facility (<http://glcfapp.umd.edu:8080/esdi>). For a geomorphologic overview and for deriving the characteristic, geomorphologic features of tsunami prone areas, terrain parameters and morphometric maps were extracted from SRTM DEM data, such as shaded relief, aspect and slope degree, minimum and maximum curvature, or profile convexity maps, using ENVI 4.3 / CREASO and ArcGIS 9.2 / ESRI software. For enhancing the LANDSAT ETM data, digital image processing procedures were carried out. With digital image processing techniques, maps can be generated to meet specific requirements, considering the tsunami risk site mapping. As a complementary tool, Google Earth Pro Software was used in order to benefit from the high-resolution 3D imageries of the coastal areas (<http://earth.google.com/>). A systematic GIS approach is recommended for tsunami risk site detection based on SRTM data as described in Figs.1 and 2 extracting geomorphometric as part of a Tsunami / Hazard Information System. The digital topographic data were merged with LANDSAT ETM data (Band 8: 15 m resolution).

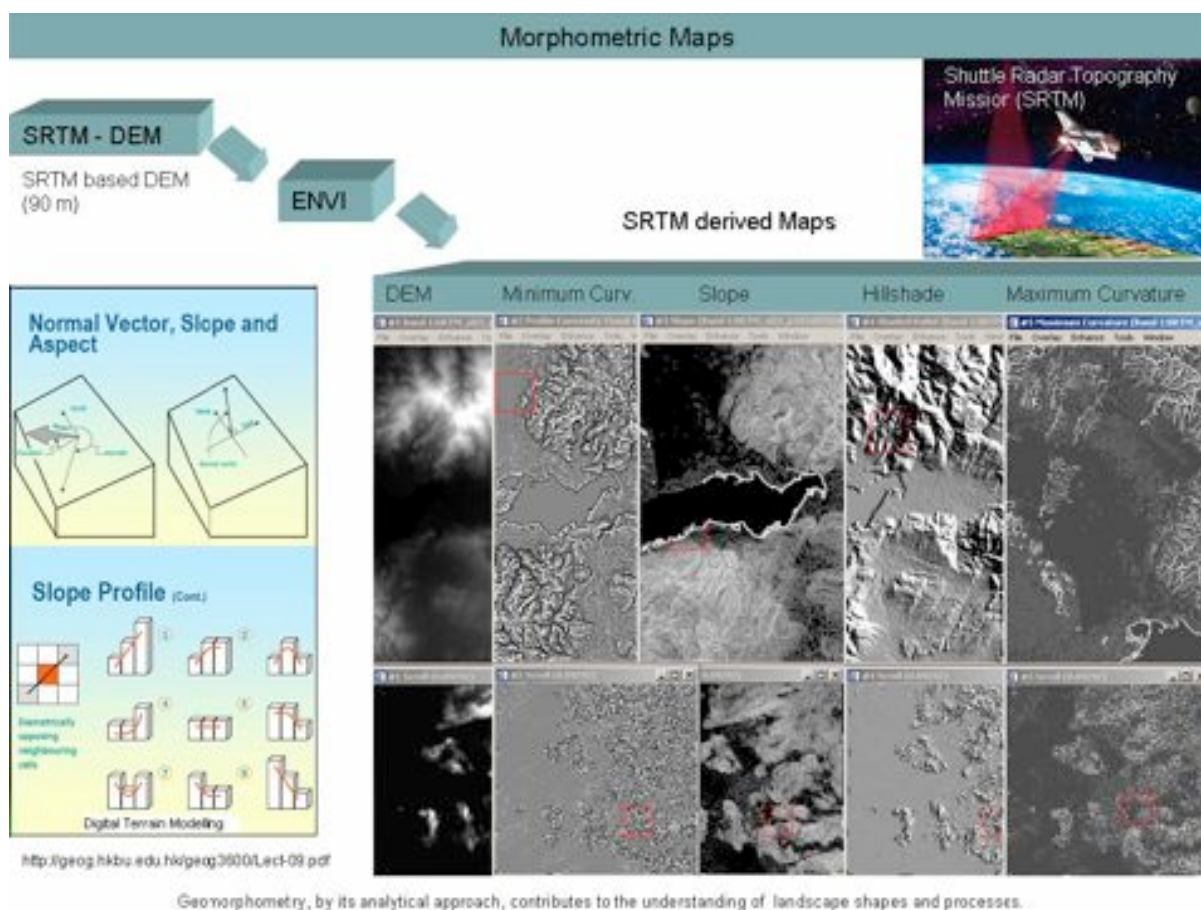


Figure 1. Deriving morphometric maps from SRTM DEM data and integration of these maps into a GIS as shown by the example of the Izmir area.

The evaluation of digital topographic data is of great importance as it contributes to the detection of the specific geomorphologic/ topographic settings of tsunami prone areas.

Evaluations of digitally processed and enhanced LANDSAT ETM imageries (merged with the pan-chromatic band for getting 15 m resolution) and high resolution imageries provided by Google Earth as QuickBird (up to 0,60 m resolution) from recently tsunami prone areas in Sumatra and Sri Lanka, have shown the existence of typical morphologic, hydrologic and lithologic properties as there are: $\frac{3}{4}$ linear, parallel, seawards oriented, erosional features related to marine abrasion, flux and reflux; $\frac{3}{4}$ remnants of tsunami floods are irregular swamps, ponds and lagoons near the coast; $\frac{3}{4}$ concentration of lagoons in a higher density; $\frac{3}{4}$ arc-shaped “walls” and “terraces” opened towards the sea, terraces and scarps parallel to the coast; $\frac{3}{4}$ fan-shape like or channel-like arranged drainage pattern; $\frac{3}{4}$ fan shaped, flat areas; $\frac{3}{4}$ broad river beds and estuary plains; $\frac{3}{4}$ seawards orientation of the slopes; $\frac{3}{4}$ sedimentary covers visible due to characteristic, spectral properties; $\frac{3}{4}$ abrasion areas visible due to characteristic morphologic and spectral properties (Theilen-Willige, 2006)

Hill shade maps for example help to identify marine abrasion platforms. A fan-shaped, flat morphology at the coasts is often related to flooding events. Aspect maps, minimum curvature and slope gradient maps contribute to the detection of arc-shaped walls and terraces oriented towards the sea.

The northern part of the Aegean Sea was chosen to investigate the potential of satellite data for the detection of traces of flood waves. The coastal areas of the Aegean Sea are investigated in order to detect typical geomorphologic and hydrologic features as described before and assumed to be related to past tsunamis. Merging morphometric maps as height, hill shade and profile convexity map from this region helps to visualize the areas being susceptible to flooding.

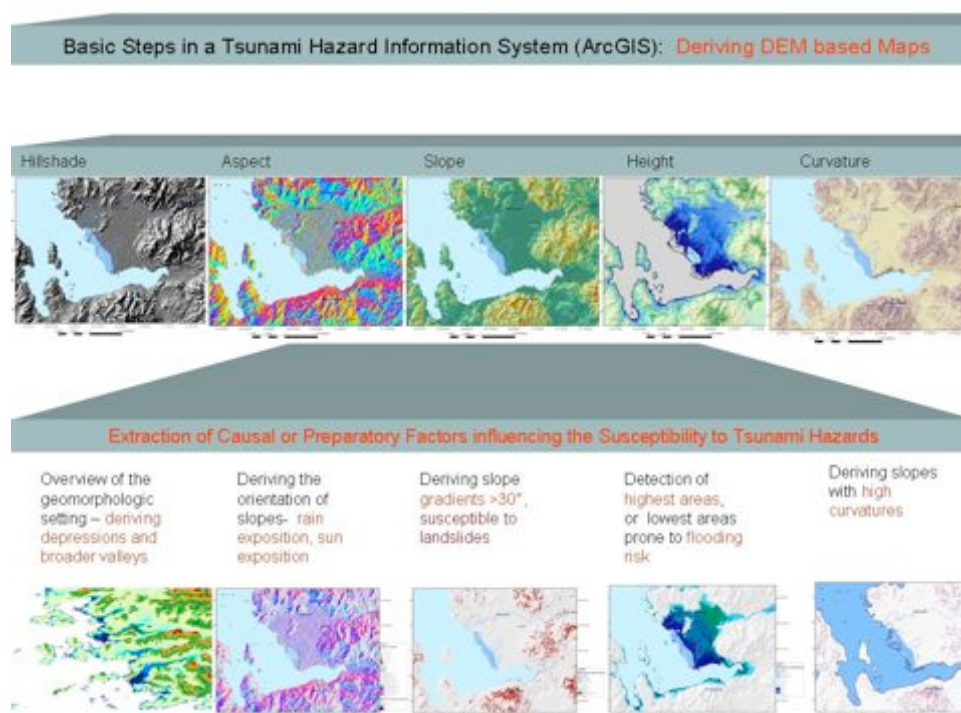


Figure 2. Deriving morphometric maps based on Digital Elevation Model (DEM) data provided by the Shuttle Radar Topography Mission (SRTM) in February 2000 in order to detect tsunami-related geomorphologic features demonstrated by the example of the Izmir area / West -Turkey

Potential risk sites for hazardous tsunami waves were identified by analyzing areas showing heights below 20 m above sea level (Fig.3). These regions below 20 m height were studied then more detailed evaluating LANDSAT ETM, QuickBird and SRTM DEM data. Investigations were focused on those areas where evaluations of SRTM , LANDSAT ETM and other geodata allow the assumption that catastrophic tsunami events might have occurred in the past and that these areas could be susceptible to flooding in future again.

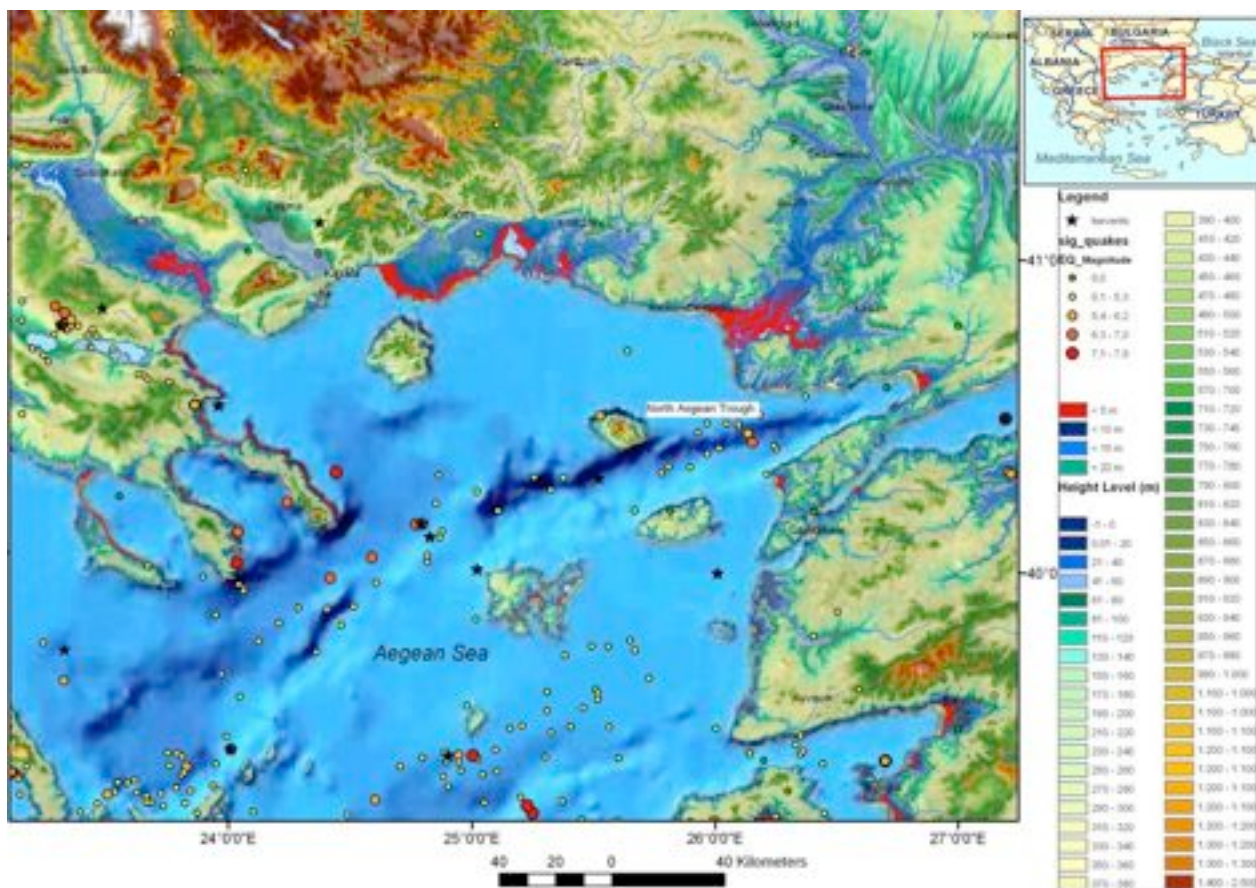


Figure 3. Earthquake and tsunami occurrence in the Aegean Sea

Tsunami data: <http://map.ngdc.noaa.gov/website/seg/hazards/viewer.htm>
 Earthquake data: http://neic.usgs.gov/neis/eq_depot/2003/eq_030814/neic_xlaf_p.html
<http://www.gein.noa.gr/services/infoen.html>
 Bathymetric map: <http://worldwind.arc.nasa.gov/>

3. GEOLOGIC AND TECTONIC SETTING

The most significant bathymetric feature of the north Aegean Sea is the North Aegean Trough (NAT), which consists of a series of deep fault-bounded basins. Those in the west have a NE trend, while those in the eastern part of the system trend ENE. The easternmost basin, the Saros trough, is also the narrowest: in its western part, south of Samothraki, the bathymetry and gravity suggest it is a half graben bounded by a large normal fault system along its northern margin (Taymaz et al., 2004). Fault plane solutions in the western part of the North Aegean Trough show mainly strike-slip faulting, consistent with right-lateral slip on NE-SW striking faults. The focal mechanisms give the impression that the north and central Aegean Sea is dominated by distributed strike-slip faulting: most of it right lateral with a NE to ENE strike. Several of the islands appear to be the uplifted footwall crests of such normal faults, and are adjacent to deep basins offshore. There is further evidence from paleomagnetism that this western region rotates clockwise relative to stable Europe. In the central and eastern Aegean, and in NW Turkey, distributed right-lateral strike-slip is more prevalent, on faults trending NE to ENE, and with slip vectors directed NE. The strike-slip faulting that enters the central Aegean from the east appears to end abruptly in the SW against the NW-trending normal faults of Greece. Tsunami hazards are well documented in the Aegean Sea. Some of the known tsunamis are presented in Fig. 3.

4. EVALUATIONS OF SATELLITE DATA FROM COASTAL AREAS OF THE AEGEAN SEA

4.1. Detection of potential hazard sites

As can be seen in Fig. 3 the susceptibility of coastal areas to flooding varies depending on their morphologic properties. This is visualized using satellite data by Fig. 4 summarizing some of the different coast types and their susceptibility to flooding – similarly to the study by Kumaraperumal et al. (2007).

Coastal Morphology Influencing Tsunami Hazard Susceptibility

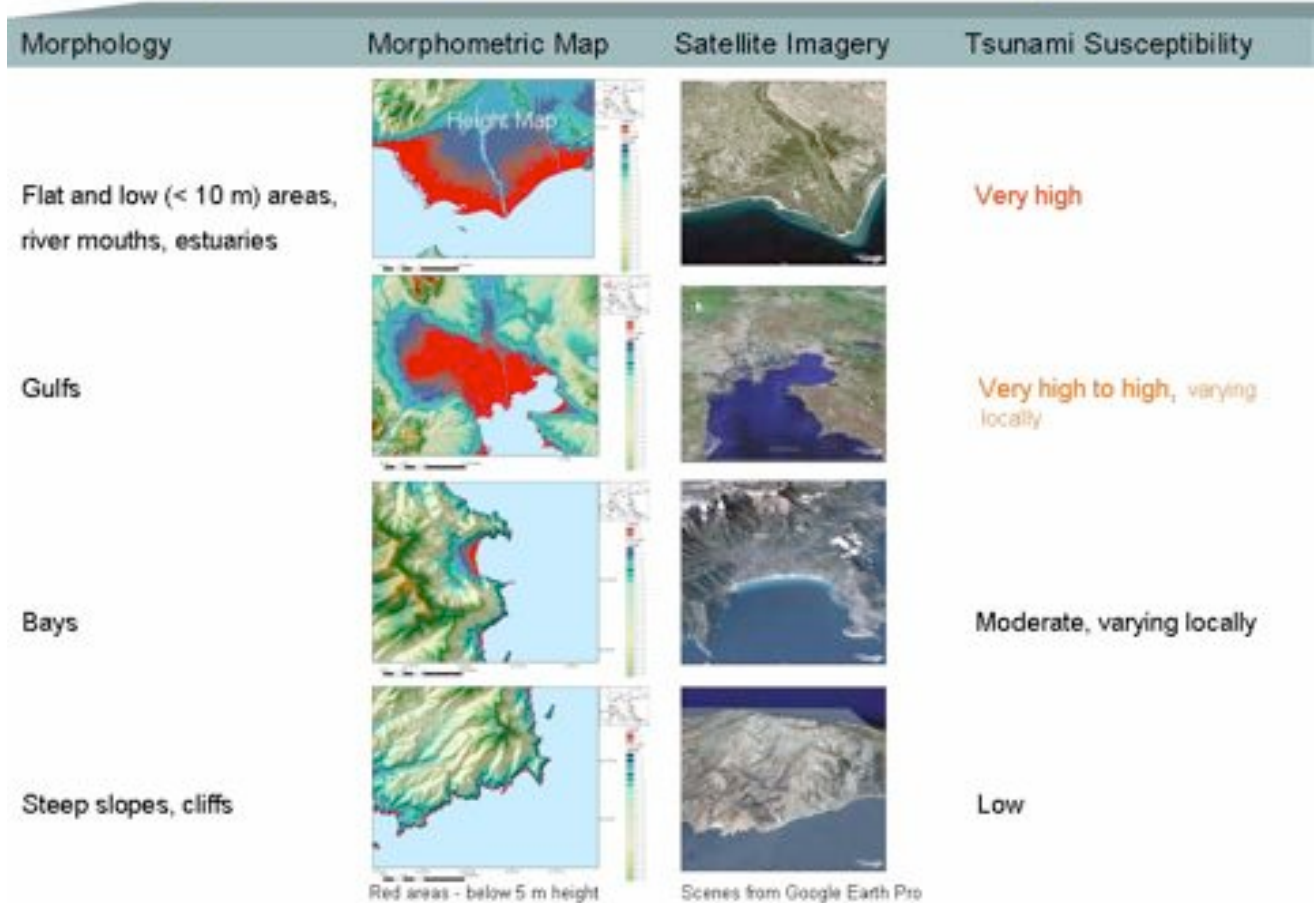


Figure 4. Coastal morphology influencing tsunami flooding susceptibility

A local increase of tsunami damage near the mouth of rivers, due to the refraction of tsunami waves with dependence on river orientation and direction of arrival of tsunami has to be considered. The extent of inundation is also determined by the angle of incidence of the tsunami surge as well as its velocity. The fluctuating surges of water could cause infilling and draw down bays and send volume of water miles inland along large coastal rivers. As larger bays and gulfs in the Northern Aegean Sea are most probable to be affected by flooding in case of catastrophic tsunami events those areas are shown in Fig. 5.

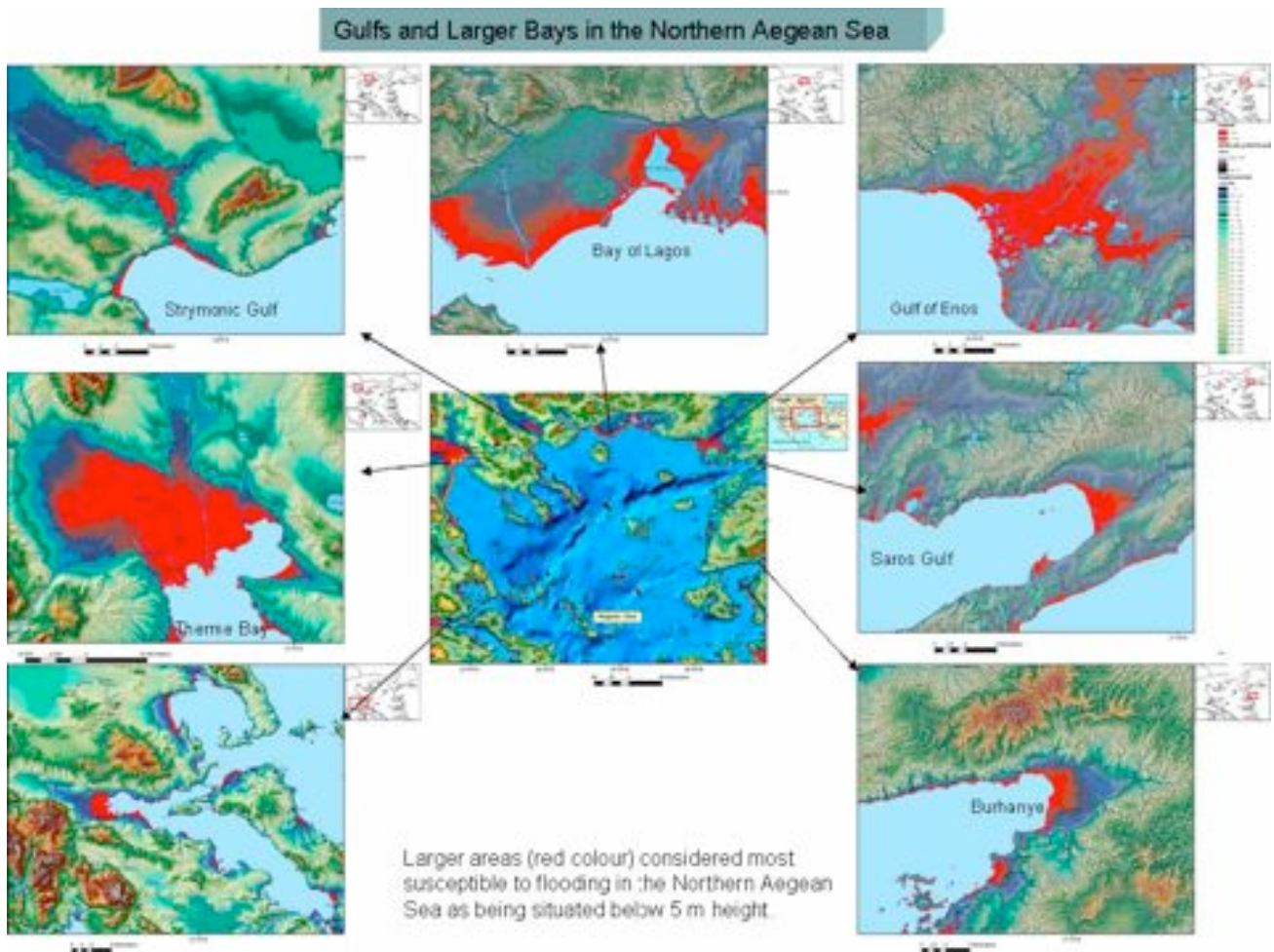


Figure 5. Extended areas with high flooding susceptibility in case of tsunami events

As example to demonstrate the potential of remote sensing and GIS methodology for the site detection of tsunami hazard prone areas is shown the area of the Bay of Lagos (Fig.6 a and b). An overlay of height levels and a profile convexity map derived from SRTM DEM data clearly shows flat and low areas forming terrace-like, morphologic features, opened towards the sea. The morphometric maps of this area (Fig.6 a) support the assumption that this area was hit by catastrophic tsunamis in the younger geologic past.

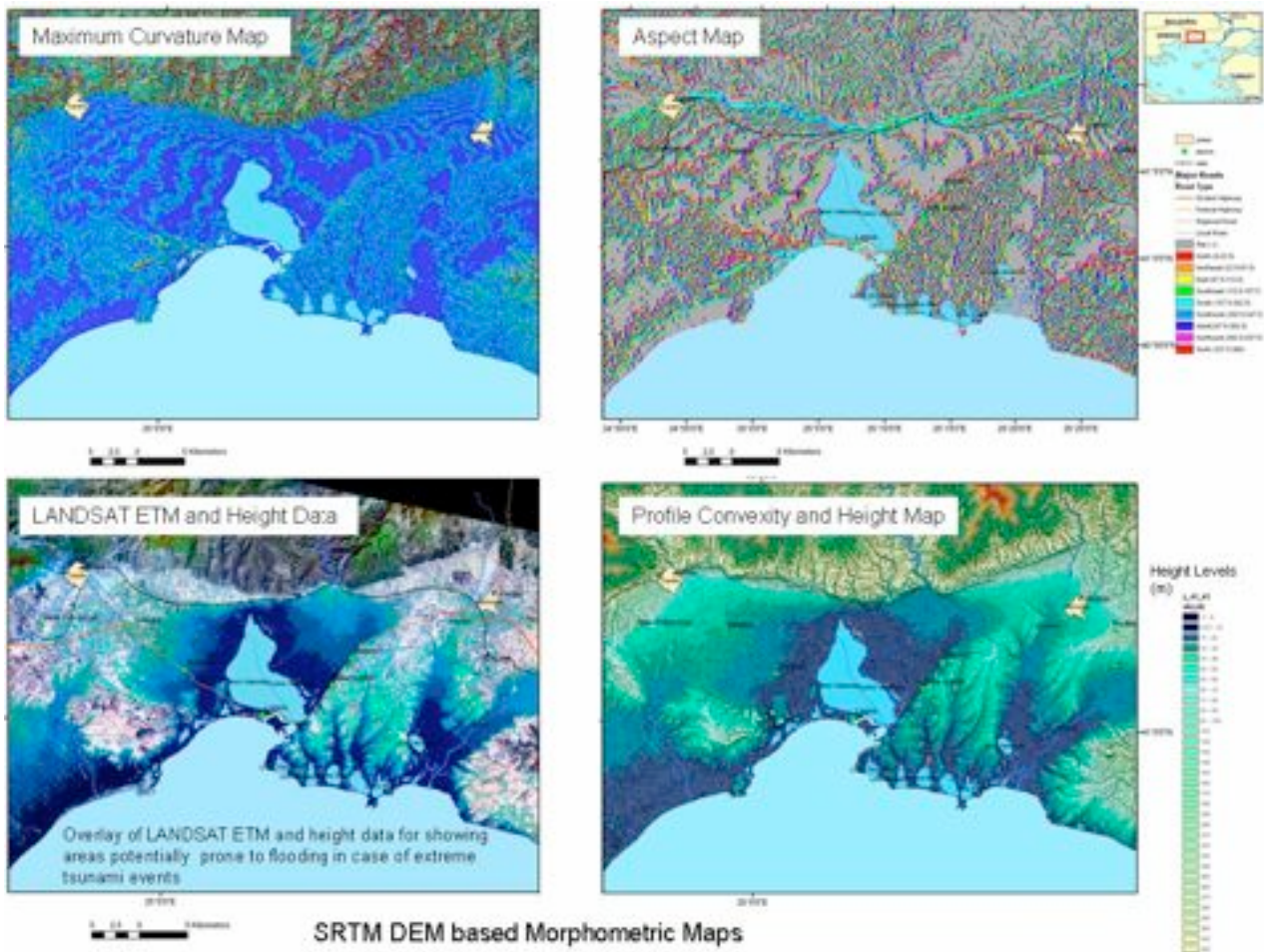


Figure 6 a. Morphometric maps of the northern coastal area of the Aegean Sea

Probable, ancient flooding waves seem to be traced by arc-shaped, terrace-like features at the coasts on the maximum curvature map, profile convexity map and aspect map. Merging the SRTM based height data with LANDSAT ETM imageries (sharpened to 15 m resolution) allows a more detailed analysis and mapping of potentially flooding prone areas. The LANDSAT ETM / height level data overlay (Fig.6 c) shows that fortunately no larger settlements, roads and railways are situated in areas below 10 m height. The minimum curvature map seems to trace marine waves.

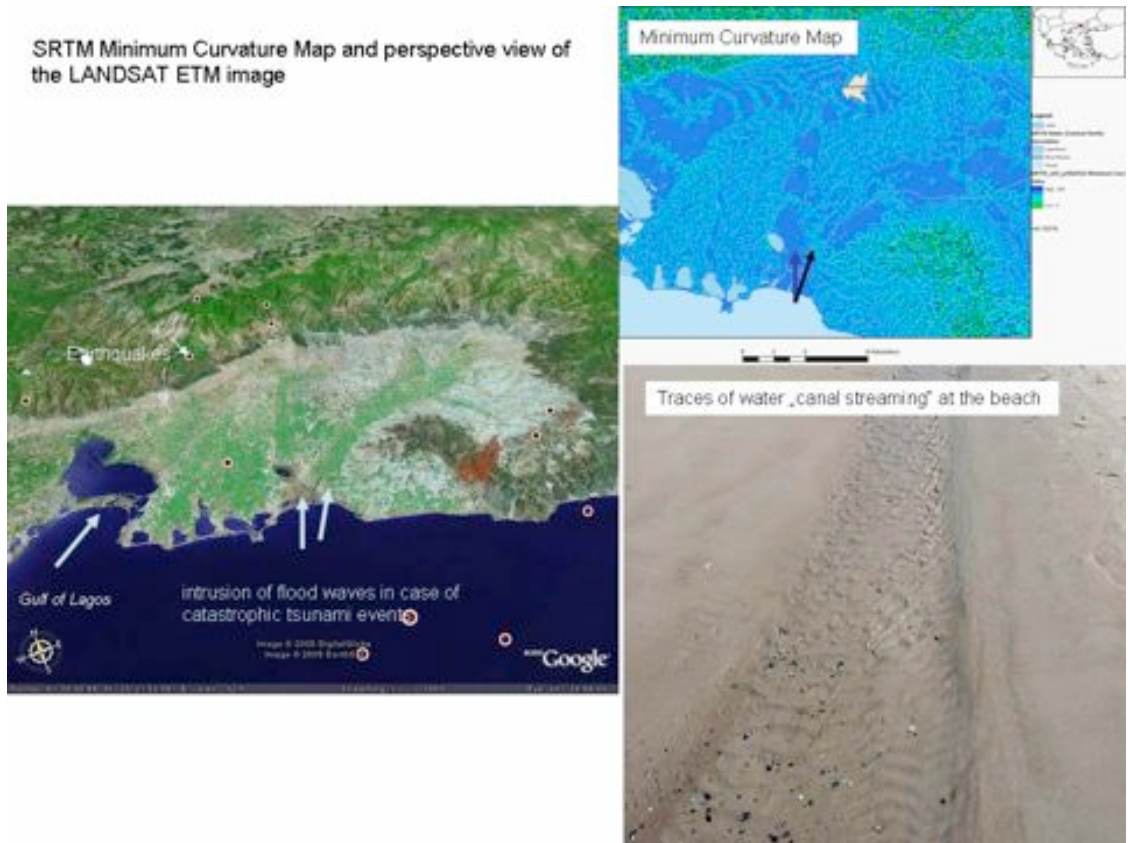


Figure 6 b. Lagos and Anadoli Bay

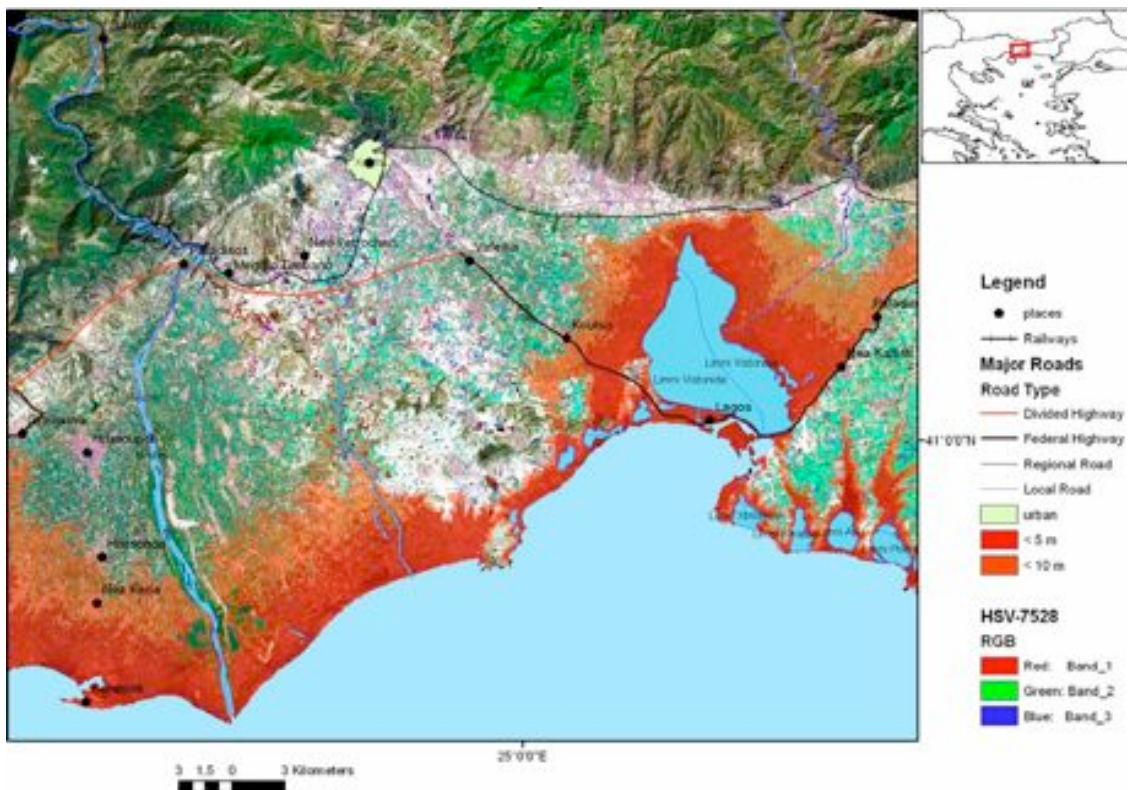


Figure 6 c. LANDSAT ETM scene merged with height data.

4.1. Evaluations of LANDAT and SRTM Data for the detection of surface-near sea water currents

An important contribution of digitally processed satellite imageries is the **visualization of surface water currents**. This might give information of those areas where flood wave energy might be focused due to the influence of coastal morphology. Evaluations of LANDSAT imageries for the detection of surface-near water currents have been carried out for the northern part of the Aegean Sea. The LANDSAT ETM image (Fig.7) visualizes the water currents and circulation in the northern part of the Aegean sea at the acquisition date (20.08.2001). The influence of the coastal morphology and of the islands on the streaming mechanisms is clearly visible. The height level information is derived from SRTM data. Areas below 5 m height are shown in red for enhancing those areas most susceptible to flooding in case of extreme tsunami events.

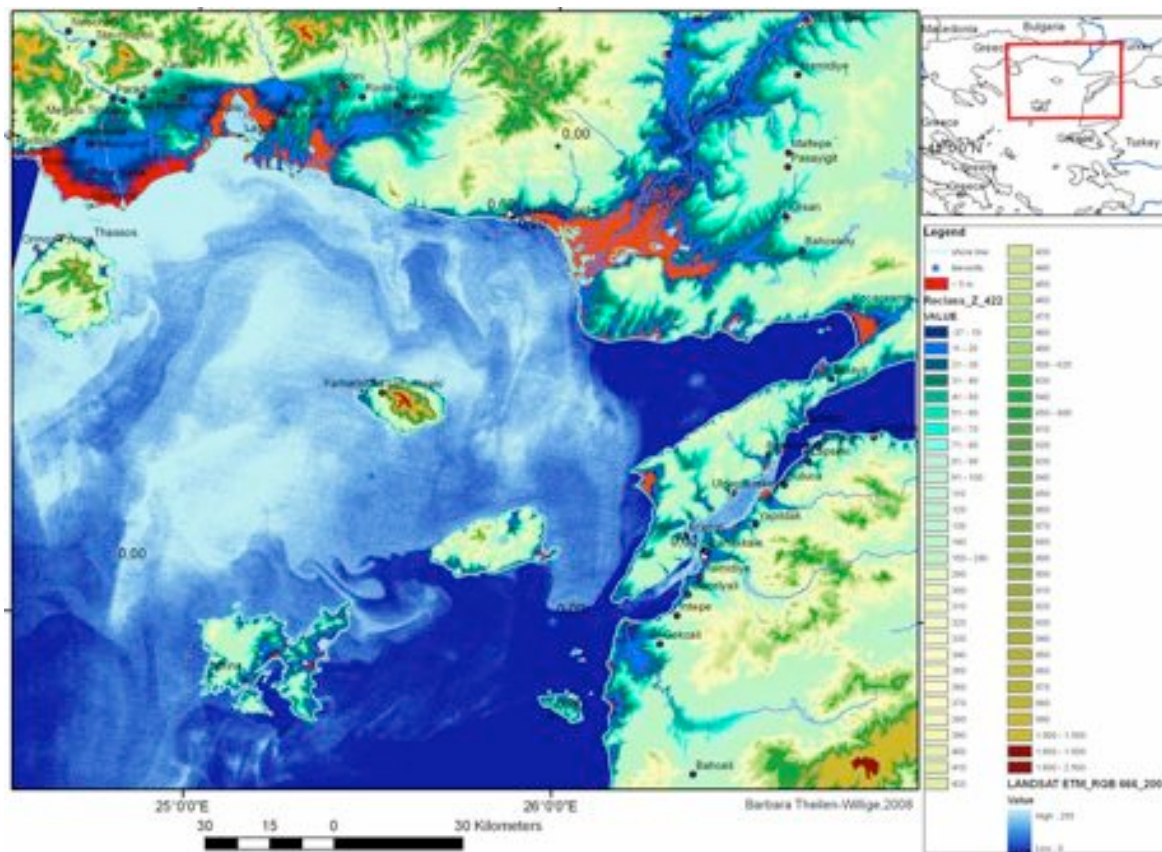


Figure 7. LANDSAT ETM image (thermal band) and height level overlay of Limnos (lower left) and Gökçeada islands
Areas below 5 m are presented in red. These areas are most susceptible to flooding

How a small island can influence water streams coming from the Sea of Marmara is shown by the next figure (Fig.8) and the influence of coastal morphology in Fig. 9. As a small island is situated directly within the water streams coming from the Sea of Marmara, it divides the water streams. This can be observed on the color-coded LANDSAT image.

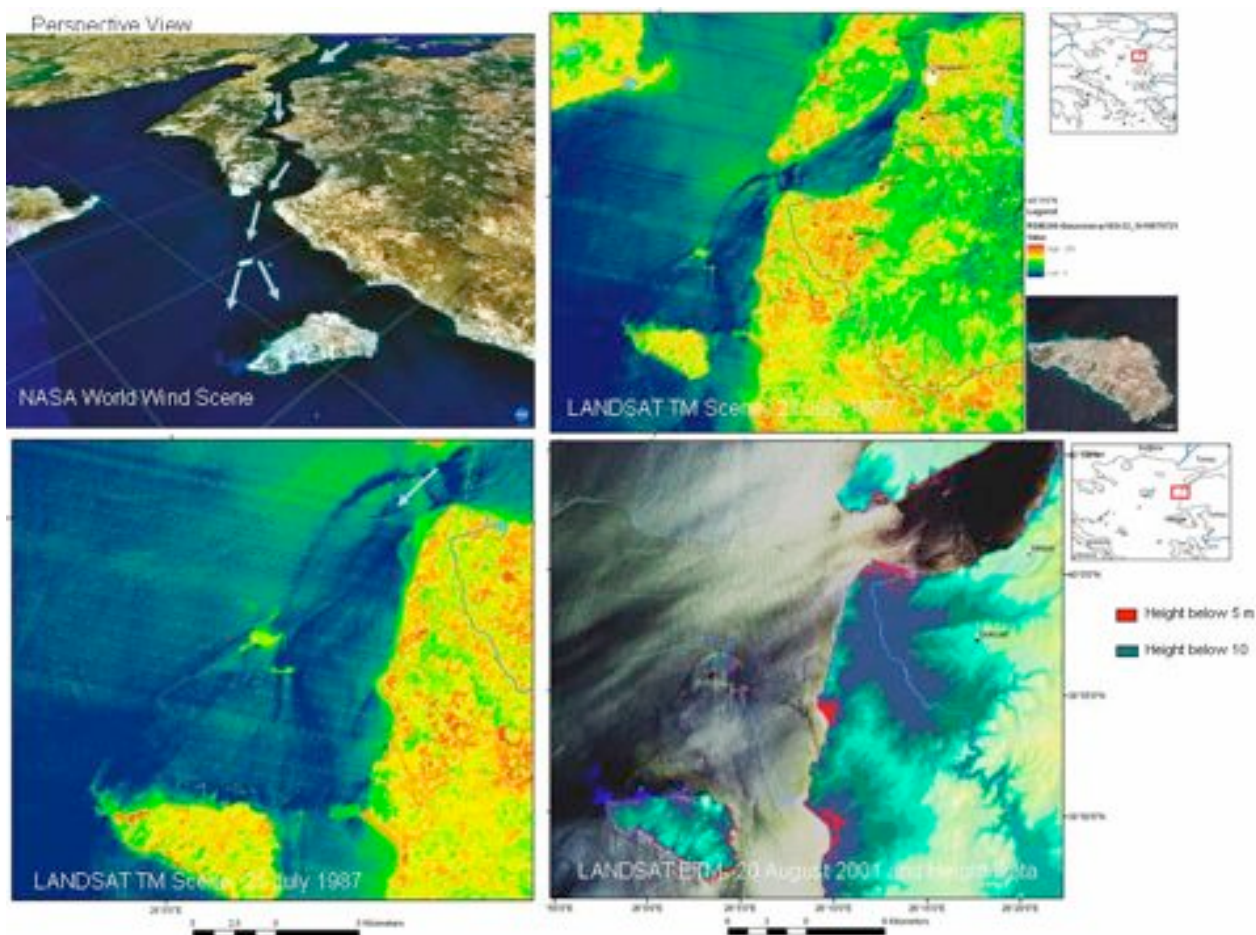


Figure 8. Influence of islands on water streaming mechanisms

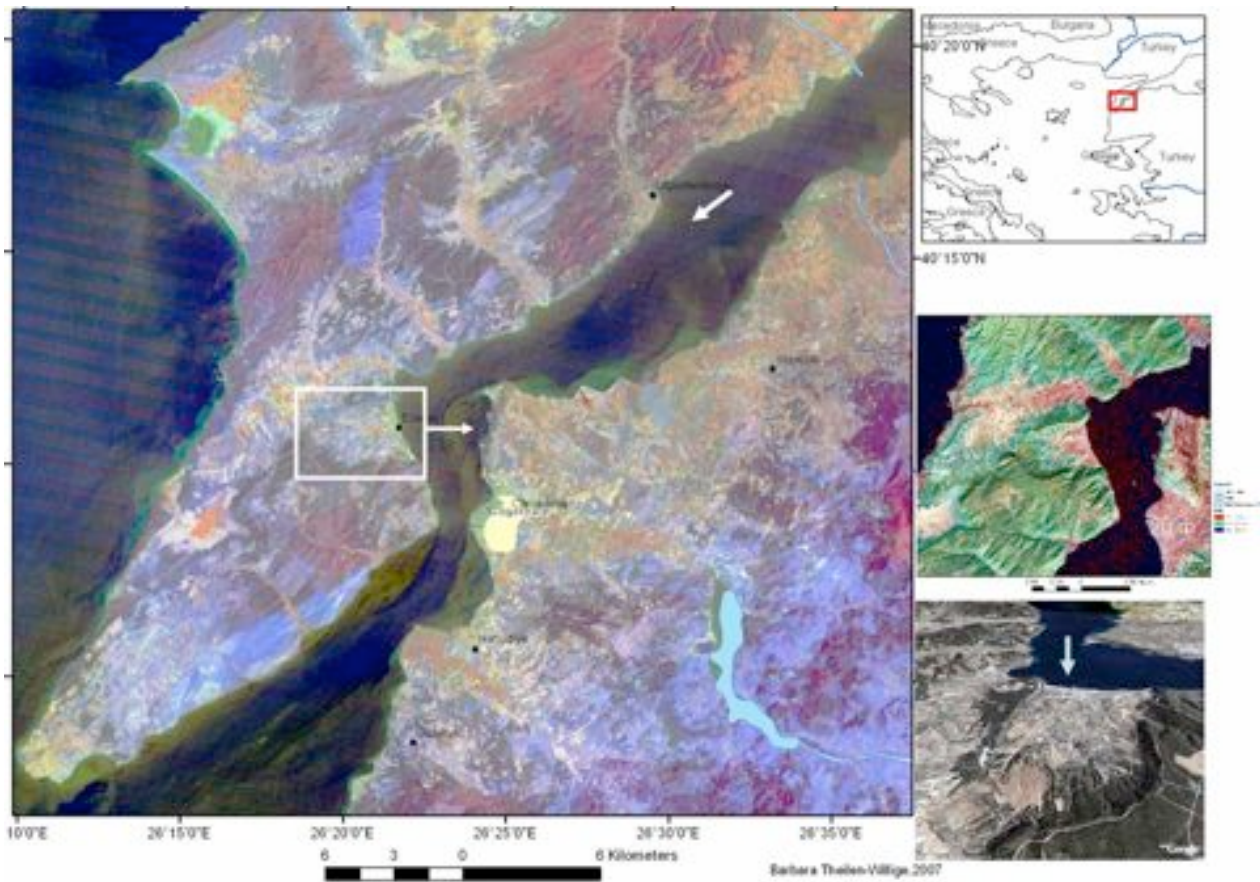


Fig.9: Areas most susceptible to flooding due to focusing effects

When calculating values below 0 m sea level based on SRTM data small sea surface height differences become visible as shown in Fig.10. Although these height differences most probably are related to wind conditions at the acquisition date such a sea surface height map contributes to a better understanding of the influence of coastal morphology on water

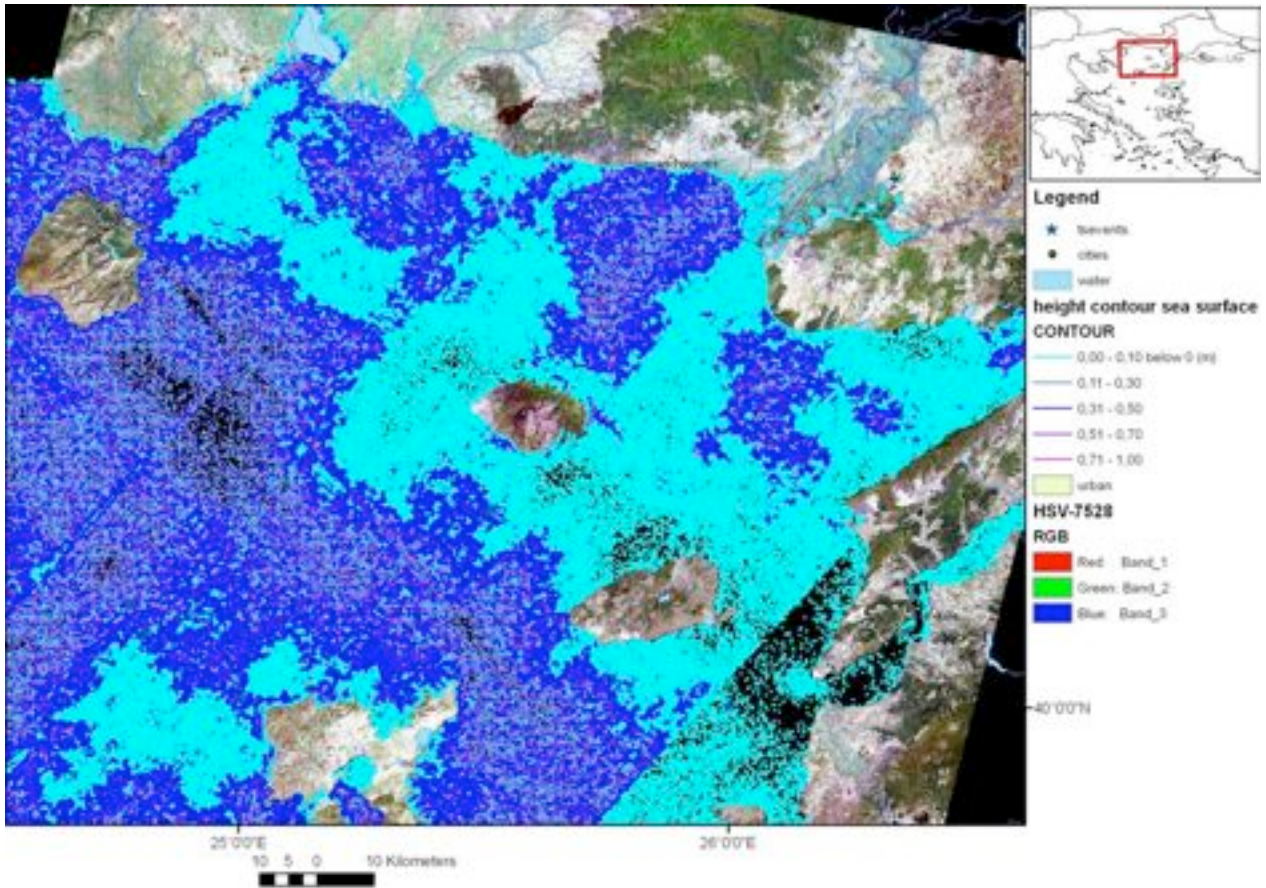


Figure 10. LANDSAT ETM and SRTM data for detecting water currents and sea surface height variations, mainly due to wind intensity and wind direction and temperature gradation

5. CONCLUSIONS

The evaluations of different remote sensing data combined with other geodata in a GIS environment allow the delineation of areas susceptible to tsunami flooding and inundation in the coastal areas of the Aegean Sea. This might contribute to the detection of future potential flooding regions. The interpretation of remote sensing data from ancient tsunami prone areas will help to a better recognition of hazardous sites in future and, thus, being one basic layer for a tsunami alert system. The findings can be converted to recommendations for the local governments such as towns and villages in order to plan disaster-reducing activities.

6. REFERENCES

- Fokaefs, A. & Papadopoulos (2004) Tsunamis in the area of Cyprus and the Levantine Sea. Geophysical Research Abstracts, Vol.6, 00858,2004, European Geosciences Union
- Gupta, R.P. 2003. Remote Sensing Geology. Springer Verlag,
- Kelletat, D., and G. Schellmann. (2001) KŸstenforschung auf Zypern: Tsunami Ereignisse und chronostratigraphische Untersuchungen. *Essener Geographische Arbeiten*, **32**, UniversitŸt Essen, Germany.
- Kumaraperumal, R., Natarajan, S., R. Sivasamy, S. Chellamuthu, S.S. Ganesh and G. Anandakumar (2007) Impact of Tsunami 2004 in coastal villages of Nagapattinam District, India. - Science of Tsunami Hazards, Vol. 26, No. 2, page 93 (2007)
- Papadopoulos, G.A., and B.J. Chalkis. (1984) Tsunamis observed in Greece and the surrounding area from Antiquity up to the present times. *Marine Geology*, **65**, 309-317.
- Taymaz, T. (2001) Active Tectonics of the North and Central Aegean Sea. Scientific Activities 2001, IT† – Faculty of Mines, XV- XXIII, Istanbul Technical University
- Taymaz, T., Westaway, R. and Reilinger, R., (2004) Active Faulting and Crustal Deformation in the Eastern Mediterranean Region, *Special Issue of TECTONOPHYSICS*, **391**, Issues 1–4, 375 pages, Elsevier Publications (20020516/18), October 29, 2004.
- Theilen-Willige, B. (2006) Tsunami Risk Site Detection in Greece based on Remotes Sensing and GIS Methods. Science of Tsunami Hazards, **24**, 1, 35-48, Address: <http://www.sthjournal.org/241/willige.pdf>
- Theilen-Willige, B. (2006) Remote Sensing and GIS Contribution to Tsunami Risk Sites Detection in Southern Italy. *Photogrammetrie, Fernerkundung und Geoinformation - PFG*, **2**, 103-114
- Whelan, F. & Kelletat, D. (2002) Geomorphologic Evidence and Relative and Absolute Dating Results of Tsunami Events on Cyprus. *Science of Tsunami Hazards*, **20**, 1, 3-18 World Wide Web Address: <http://library.lanl.gov/tsunami/ts201.pdf>
- Wijetunge, J.J. 2006. Tsunami on 26 December 2004: Spatial Distribution of Tsunami Height and the Extend of Inundation in Sri Lanka. Science of Tsunami Hazards, 24, No. 3, page 225-239
- Yalciner, A. C., Alpar B., Altinok Y., zbay I., Imamura F. (2001) Tsunamis in the Sea of Marmara: Historical Documents for the Past, Models for Future" Special Issue of Marine Geology, V: **190**, 2002, 445-463

Yalciner, A. C., Pelinovsky E., Talipova T., Kurkin A., Kozelkov A., and Zaitsev A., (2004) Tsunami in the Black Sea: Comparison of the historical, instrumental, and numerical data. *J. Geophys. Res.*, **109**, C12023, doi: 10.1029/2003JC002113.

Yolsal, S. and Taymaz, T. (2005) Potential source regions of earthquake triggered tsunamis along the Hellenic and Cyprus arcs, Eastern Mediterranean. *International Symposium on the Geodynamics of Eastern Mediterranean: Active Tectonics of the Aegean*, Kadir Has University, Cibali Campus, 15-18 June 2005.

Satellite Data:

World Wide Web:

<http://glcfapp.umiacs.umd.edu:8080/esdi/index.jsp>

<http://worldwind.arc.nasa.gov/download.html>

<http://earth.google.com/>

Shape files:

<http://map.ngdc.noaa.gov/website/seg/hazards/viewer.htm>

http://www.cipotato.org/diva/data/DataServer.asp?AREA=DZA&THEME=_adm

LARGE BOULDERS ALONG THE RABAT COAST (MOROCCO); POSSIBLE EMPLACEMENT BY THE NOVEMBER, 1st, 1755 A.D. TSUNAMI

Nadia Mhammdi, Fida Medina

Université Mohammed V-Agdal, Institut Scientifique, Département des Sciences de la Terre, Av. Ibn Batouta, B.P. 703 Agdal, Rabat, Morocco.

mhammdi@israbat.ac.ma; medina@israbat.ac.ma

Dieter Kelletat

Universität Köln, Institut für Geographie, Albertus Magnus Platz 1, Koeln, Germany.

dieter.kelletat@t-online.de

M'Fedal Ahmamou, Lamiaa Aloussi

Université Mohammed V-Agdal, Faculté des Sciences, Département des Sciences de la Terre, Av. Ibn Batouta, B.P. 1014 R.P., Rabat, Morocco.

ahmamou@israbat.ac.ma

ABSTRACT

The rocky coastline south of Rabat (Morocco) shows a large number of boulders lying upon the lithified dune system. The boulders, of 4-100 tons, may be single, in imbricated sets, or forming clusters and ridges. Several of the boulders were lifted and overturned, thus showing pool apertures downwards. Transport distance is generally decametric because of the surface roughness, but it can reach 300 m in flat areas. All boulders have been detached from their initial position at the fractured front of the active cliff. Quantification with the help wave hydrodynamics and rock displacement mechanics shows that dislodgement and transport of these boulders were accomplished rather by tsunami than by storm waves. Although no dating was attempted, post-emplacement bio-erosion by littorinids and the absence of any erosional features below the boulders suggests that they were emplaced during the 1st November 1755 AD Lisbon tsunami.

Key words: Morocco, Rabat coast, tsunami, boulders, 1755 Lisbon earthquake.

1. INTRODUCTION

The northwestern Moroccan coastline is fully exposed to the Gulf of Cadiz (Fig. 1), where the boundary of the North African and European plates becomes convergent near the Goringe Bank (e.g. Buform et al., 2004; Stich et al., 2005). This zone, probably one of the most dangerous seismic and tsunamigenic areas in the world, is the source of the Lisbon earthquake (M=9.0) on November, 1st, 1755AD, as well as of other historical events (216-209BC, 881AD, 1731AD), that led to partial destruction of some Moroccan and south-western Iberian coastal cities (Campos, 1991; Elmrbet, 2005). This seismogenic / tsunamigenic area continues to be active, as attested by the occurrence of the large earthquakes of 28 February 1969 (M=7.3), 26 May 1975 (M=7.9), which generated small tsunamis (Baptista et al., 1992; Heinrich et al.; 1994), and 12 February 2007 (M=6.3), strongly felt in Morocco. The calculated return period of tsunami generation is of 200 years in some oceanic sectors around 36°N 10°W (El Alami and Tinti, 1991).

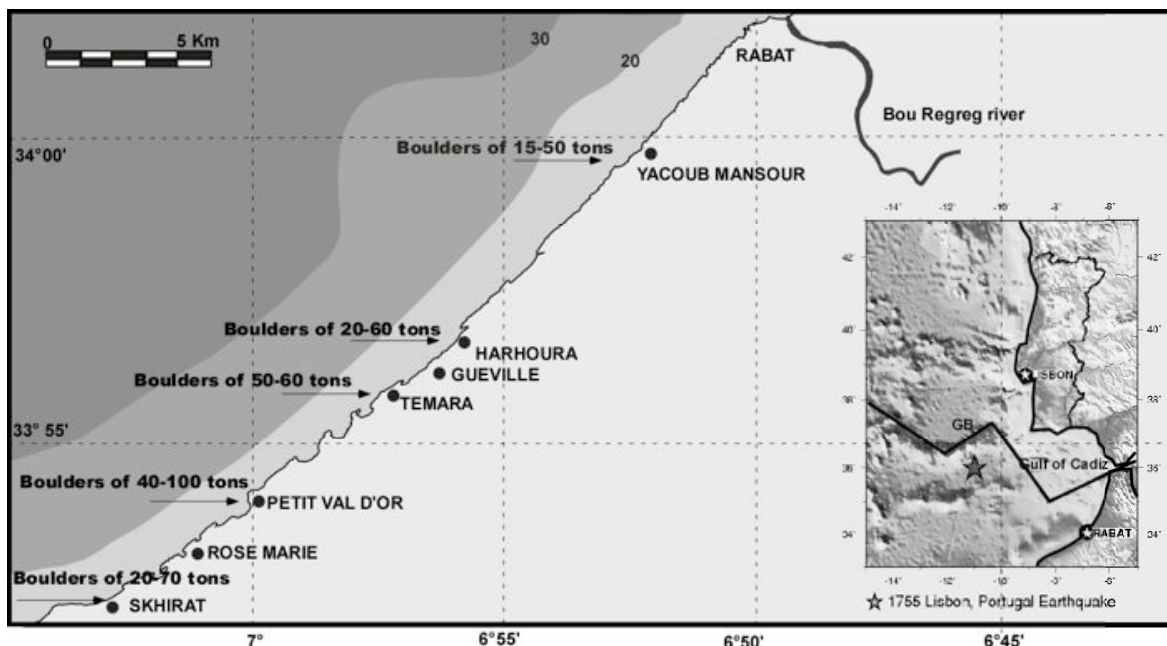


Fig. 1. Map of the coastal area south of Rabat and location of the observation sites (simplified from Milliès-Lacroix, 1974). Inset: map of the Gulf of Cadiz area showing the morphology of the sea bottom and location of the epicentre of the 1755 AD Lisbon earthquake (star). Freely licensed from USGS.

One of the most spectacular effects related to the tsunamis of the Gulf of Cadiz is the displacement of boulders of several tons along the shoreline. Such boulders have been observed in southern Spain at cape Trafalgar (Whelan and Kelletat, 2005) and in Portugal, west of Lisbon (Scheffers and Kelletat, 2005). In Morocco, despite detailed studies on the Quaternary coastal deposits (Guilcher and Joly, 1954; Gigout, 1957; Akil, 1980 among others), only Gigout (1957, p. 10-11, plate II, Figs 3-4), described single boulders in the Rabat coastal area, and interpreted their displacement and overturning as related to storms. On the basis of literature published on Iberia, and within the context of general interest in tsunami research after the December, 26th 2004 catastrophe in the Indian Ocean, we re-visited the coastal area south of Rabat several times during 2007 in order to investigate the existence of comparable tsunami-related boulders. The first results are presented in this paper.

In the following sections, we first review the geology and morphology of the Rabat coastal area in order to set the physical environment, and then we describe the boulders and the style of their arrangement, and discuss the factors that influenced their emplacement according to wave dynamics and transport physics.

2. GEOLOGY AND MORPHOLOGY OF THE COASTLINE NEAR RABAT

The coastal area south of Rabat is dominated by a superimposed dune system and coastal marine deposits of end-Ouljian (70,000 years BP) to present age (Gigout, 1957; Akil, 1980; Saaidi, 1988). This dune system is developed upon the Palaeozoic basement of the western Meseta (Milliès-Lacroix, 1974). A transversal section shows the main morphological elements, which consist of (Fig. 2): (i) an inactive cliff; (ii) a more or less large depression (locally named *Oulja*) with recent beach and older continental deposits; and (iii) the lithified coastal dune system.

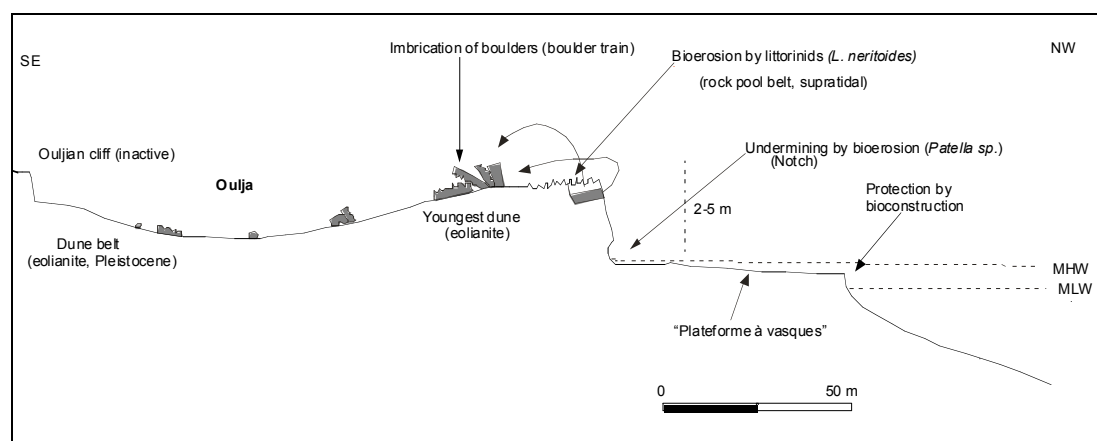


Fig. 2. Schematic transversal section of the Rabat coastal area showing the main morphological units and the type of boulder arrangement. Inspired from Guilcher and Joly (1954), Gigout (1957) and Akil (1980).

According to Gigout (1957), a typical section of the Quaternary deposits of Témara beach comprises, from older to younger (Fig. 3 A): (i) a post-Ouljian consolidated dune system, with generally an eroded top, overlain by (ii) a red clay level, rich in continental Gastropods, capped by (iii) a decimetric-scale grey limestone-sandstone (Flandrian / Mellahian; 5,000-6,000 years BP) which shows the same palaeontological content than the present beach. The latter are overlain by either a *kjoekenmoeding* or by the present-day sand. More recently, Akil (1980) mapped a total of 14 marine and continental formations, the superimposition of which was interpreted as related to alternating episodes of sea level changes. The detail of these subdivisions will not be exposed here because the complex stratigraphic issue is beyond the purpose of this paper. The seaward ridge, consisting of end-Ouljian and post-Ouljian dune complexes separated by Soltanian red clays, most probably belongs to the younger Pleistocene, stade 5e or even 5a. The dune base several meters below sea level points to a sea level of this position or lower during dune accumulation.

Morphologically, the coast south of Rabat consists of relatively small sand beaches (Temara, Sables d'Or, Skhirate...) separated by rocky cliffs and lapiazed platforms (south of Temara, Miramar, Guéville). This area shows great biodiversity (e.g. Lambert, 1985), with several species that contribute to the evolution of the landscape by their constructions or their bioerosional processes, as shown in other areas, especially around the Mediterranean (Kelletat, 1997).

As described by Guilcher and Joly (1957), the morphology of the coastal dune system can be subdivided into two types, depending on the nature of erosional mechanisms: (i) a generally flat "dissolution-driven type" (we use the original term of Guilcher and Joly although we consider that there is no dissolution of limestone in sea water), and (ii) a more abrupt mechanically-driven type.

The "dissolution (see above) type" comprises several zones:

Lapiez and pools: a very significant aspect of the surface in reach of sea water splash and spray is a dark colour and numerous pits, potholes or *marmites*, pools with very sharp rock pinnacles in between (*lapiez*), the depth of which may reach 1.5 m in places (Fig. 3 B, C). The deepening and widening of the pools was interpreted by Guilcher and Joly (1957, p. 86) as related to dissolution (see above) by water, not to mechanical erosion; however, they could be only related to bio-erosion by littorinids of the species *Littorina neritoides* L. – (Fig. 3 D), very common in the Moroccan coast (Lambert, 1985) –, grazing on endolithic algae (Cyanophyceae and Chrolophyceae) as described by Kelletat (1997) and others. Measurements of the intensity of bio-erosion on these carbonate rocks in other areas have resulted in 1-2 mm/year (e.g. Trudgill, 1987), but it is not possible to determine the number of generations of rock pools with flat bottoms and sharp notches that have been developed and destroyed by the grazing process of the littorinids. There is no doubt that these bioerosional features are of younger Holocene ages, when sea-level was close to the modern one and seawater spray and splash again reached the eolianite surface. Some remnants of old red soils or even caliche point to an old soil surface on the dune belt, most probably from the time of a lower sea level during the youngest Pleistocene.

"Plateforme à vasques": seaward of the lapiez zone appears a 10 to 40 m wide platform that has been cut out of the eolianite (Fig. 3 E), comprising large pools which are generally 25 cm deep, bounded by narrow crests and rims with bio constructions by barnacles and vermetids. This platform may display steps up to 50 cm in height, pouring seawater into each other, and is bounded by the mean high tide cliff. Its lower boundary appears at half tide. Between the two cliffs, and in particular the seaward fringe of the platform, where the stronger waves break, the platform shows significant bio construction and no fresh signs of plucking or quarrying. We interpret this platform as the result of coastal abrasion and bio-erosion in notches by limpets (*Patella* sp.) during the higher Holocene (Mellahian; 5,000-6,000 BP) sea-level, which – according to the levelling topography of the platform – should be rather stable, and at the modern level for a longer time of the Younger Holocene.

Area of break-up of the Plateforme à vasques. This area, only exposed at low tide, is characterized by basins that are deeper than those of the plateforme à vasques (25-80 cm), and is bounded seawards by the low tide cliff.

In the mechanical-driven type, the seaward slope of the dune system breaks and forms a generally highly fractured high tide cliff, with large blocks tilted seawards, or fallen at the base of the cliff (Fig. 3 E). However, the *plateforme à vasques* and the basin break-up areas are present although with a smaller width

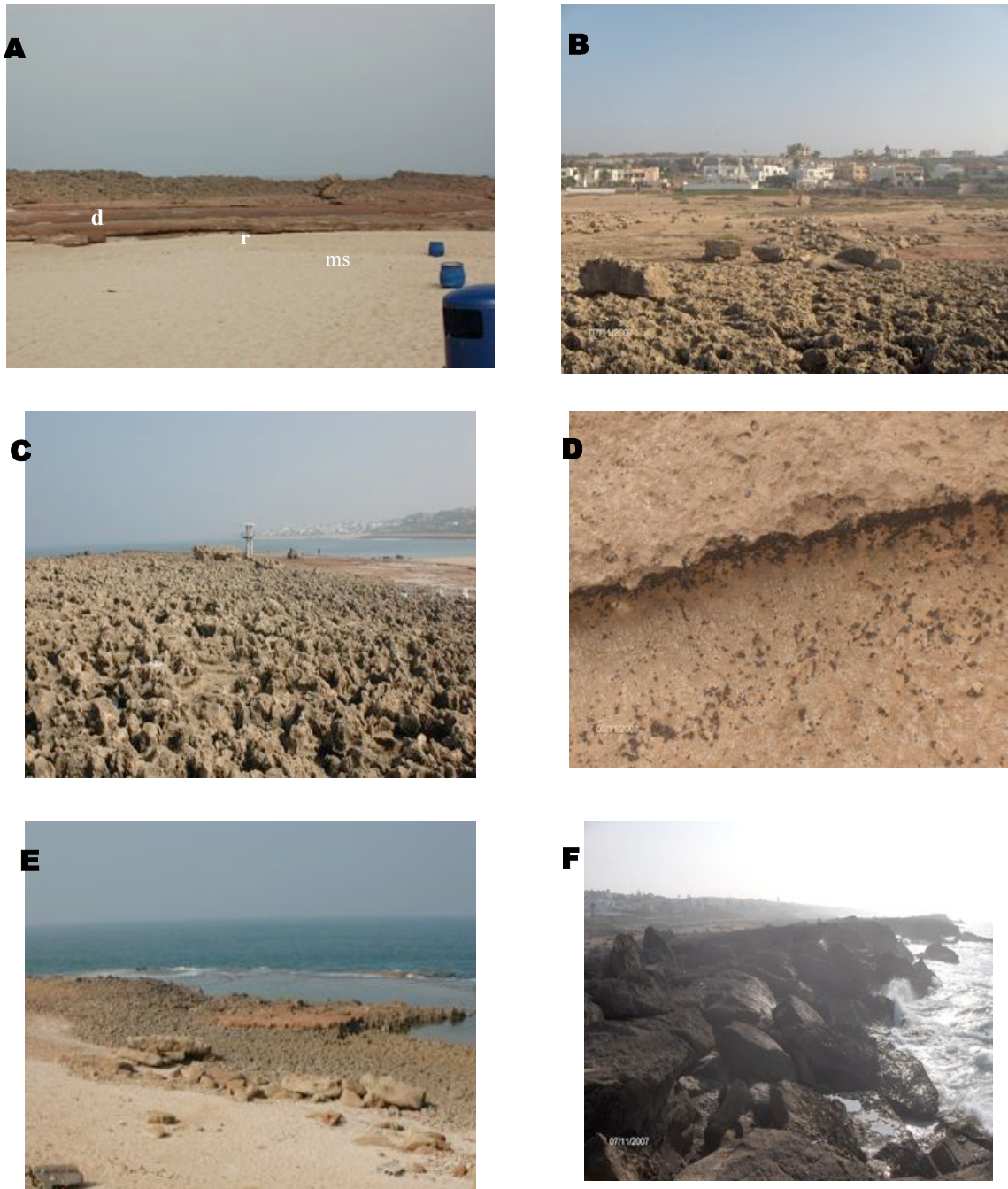


Fig. 3. Some geological and morphological features of the coastal area south of Rabat. **A**, Main Quaternary formations at Témara; successively from the foreground: present-day beach sands, then Mellahian (5,000-6,000 years BP) marine sandstones (ms), overlying red clays (r) and the lithified coastal dune (d). View to the northwest. **B**, successively from the foreground: lapiez, *Oulja* depression with boulders, and inactive cliff in the background behind the constructions at Harhoura (view to the south-east); **C**, Lapiez landscape at Temara (view to the north); **D**, example of a pool showing a concentration level of littorinids at Témara; **E**, Promontory of a partly submerged platform at Témara (view to the southwest); **F**, Highly fractured cliff in the dune belt at Harhoura (view to the southwest).

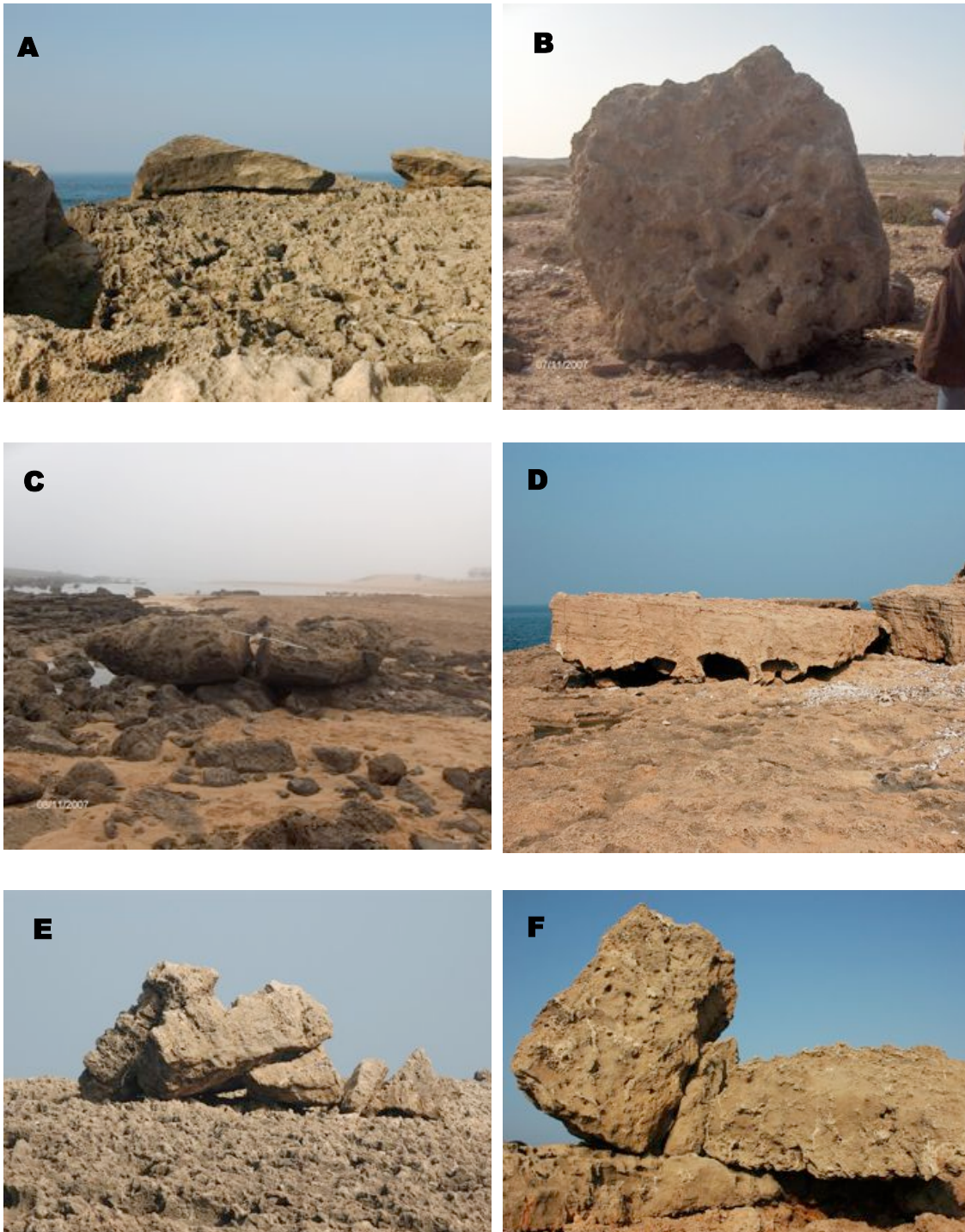


Fig. 4. Most conspicuous examples of boulder arrangement observed along the Rabat coast. **A**, Single boulders laying on cliff top at Harhoura; **B**, single fragment at Skhirate transported over 300 m; **C**, a large boulder dislocated into two fragments at Petit Val d'Or (view to the north); **D**, Two overturned boulders at Témara, showing pool openings downwards (view to the north); **E**, blocks in clusters at Harhoura (view to the southeast); **E**, **F**, trains of imbricated boulders at Témara (E) and Harhoura (F), view to the northwest in both.

3. THE BOULDERS

A striking aspect of this coastline of more than 40 km in length is the occurrence of large boulders upon the coastal formations, especially eolianite. Observation of aerial photographs shows that they extend from the southwest of the city of Rabat (municipality of Yacoub El Mansour) to Skhirat plage. As our study is preliminary, the description of the boulders is mainly qualitative, since we have just noted the dimensions and the weight of the largest blocks, and the maximum transport distance. The statistical orientation of their axes is under study.

Generally, the shape of the boulders is platy (Figs. 4 and 5). Their maximum length (A-axis) reaches 8.4 m at Val d'Or, and their weight ranges from a few tons to 100 tons. A weight of 20-30 tons is general for the larger ones, nearly all along the coast. Approximate weight was calculated using a density of 1.54-1.715 (Asebriy et al., 2007).

These boulders lay in cliff-top or landward slope (Fig. 4 A), in the landward following swale or even several meters uphill on the next eolianite ridge (Fig. 3 B). The distance to the active cliff is from a few meters to about 300 m (Fig. 4 B), and the height above high water, i.e. the rate of vertical transport, may reach more than 5 meters.

Several types of arrangement were observed:

- Single boulders (Fig. 4 B), which may be fractured by probable vertical slamming (Fig. 4 C). Some of them have been displaced in their original position, i.e. with the rock pool topography on the upper surface, whereas others have been overturned and show the rock pools at their base, with the openings to downwards (Fig. 4 D).
- Imbricated boulder trains, with up to 7 platy boulders leaning one on the other, steeper inclined to seaward (Figs. 4 E, F and 5 A).
 - Large chaotic clusters (Fig. 5 B), or, more rarely, ridges.

However, the amount and arrangement of the boulders are quite variable from one site to another:

(1) At Harhoura, the boulders are either scattered or arranged in small clusters; maximum displacement of a block is 150 m (Fig. 3 B).

(2) Southwards, Témara beach shows beautiful examples just beside the promenade alley, which is almost 2 km long. Here, the boulders may be single, imbricated, or in clusters. Maximum estimated weight is 50-60 tons. The horizontal displacement towards the continent is small (20 m), but the blocks are located at relatively high altitude (5 m), as shown in Figures 3C and 4E.

(3) The Petit Val d'Or shows the most spectacular features. In this lagoon-like beach, the boulders are very numerous and occupy a ridge of ca. 500 m x 60 m = 30,000 m² (Fig. 5 B). Maximum weight and displacement of the boulders are respectively 100 tons and 150 m. The boulders show all types of arrangement, and imbrication occurs along N110 and N160 trends (Fig. 5 A). To the south, this lagoon connects with the sea by a swale, the elevated shoulders of which also show isolated boulders, some of which reach 70 tons, are overturned, and located at relatively high altitude (2 m).

(4) In the southern area of Skhirat plage, we also observed a ridge of relatively small blocks which are isolated or imbricated along a N130 direction. Here, a 4 ton block was displaced as much as 300 m from the shoreline, along a flat platform (Fig. 4 B).

–

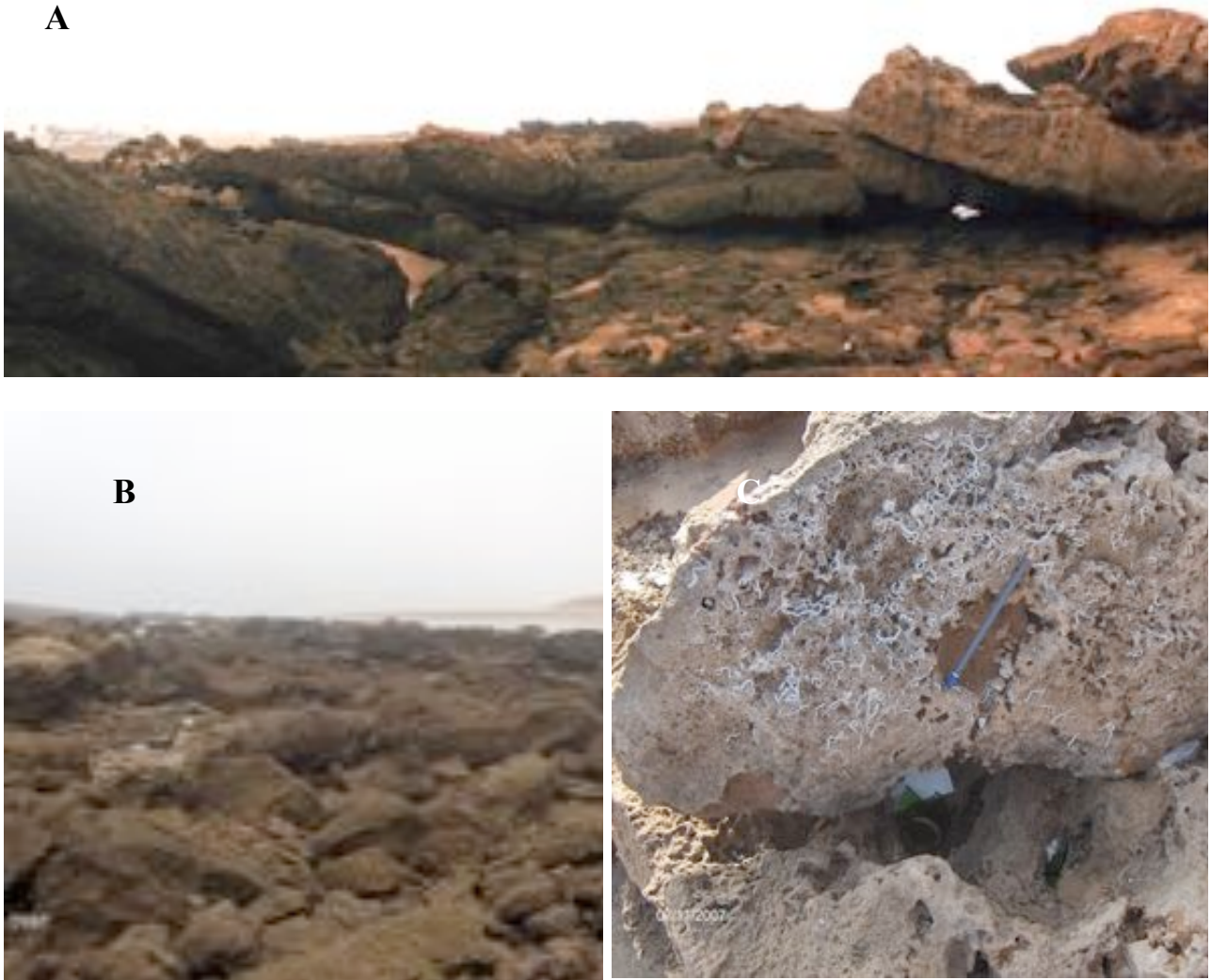


Fig. 5. A, Spectacular train of seven imbricated platy boulders at Petit Val d'Or, the uppermost being overturned, with the pool openings to downwards (view to the southwest); **B**, chaotic assemblages of blocks at Petit Val d'Or (view to the north); **C**, boulder with vermetids at Témara, attesting for uplift and transport from an infratidal area.

4. INTERPRETATION / DISCUSSION

4.1. *Provenance of the boulders*

As the lithology and morphology of most boulders is identical to that of the coastal eolianite, their source is the fractured rock pool belt close to the active cliff (Fig. 3 F), and their way of transport always is to the SE, which means perpendicular to the general coastline trend. Some boulders display small vermetids (Fig. 5 B), carvings of sea urchins or borings of bivalves (*Lithophaga* sp.), documenting their dislodgement from an area below sea-level; however, most of the boulders derive from the fractured cliff top itself, and only in the case with no signs of bio-erosion and rock pools on them, their sources are the positions of cliff rock below the rock pools belt, i.e. in the lowermost sections of the profile.

The amount of displaced boulders in a given area seems to be directly related to the density of fractures in the nearby active cliff. Thus, highly fractured cliffs as those at Harhoura (Fig. 3A) or Petit Val d'Or, would have provided more boulders than Témara or Skhirat.

4.2. *Emplacement of the boulders*

The emplacement of large boulders on shoreline platforms has been a matter of debate concerning the phenomenon to which it is related (hurricane or tsunami), especially for old unobserved or undocumented events (see discussion in Nott, 2003 and Noormets et al., 2004). Modelling of wave and tsunami hydrodynamics and rock displacement mechanics show that large waves as well as tsunami can lead to the detachment of a block from its cliff rock because the pressure may be very high, reaching 130 t/m^2 for a breaking wave, 70 t/m^2 for a tsunami (Noormets et al., 2004); however, its lift, overturning and emplacement at a distance can only be accomplished by tsunami waves because they yield greater energy and act during a longer time. In this section, we review the mechanical aspects related to boulder dislodgement and transport in order to understand the emplacement mechanisms of the Rabat boulders.

4.2.1. *Dislodgement*

First, the role of breaking waves in the dislodgement of the boulders can be assessed using the general formula of wave breaking (see Noormets et al., 2004, p. 47):

$$H_b / h_b = 0.72 + 5.6 \tan \beta \quad (1)$$

where H_b is the height of the breaking wave, h_b is the water depth at the breaking point and $\tan \beta$ is the bottom slope. Above a flat bottom ($\beta = 0$), waves will break if water depth is 1.39 of their height. Therefore, an 18 m-wave will break in about 25 m of water depth, or an 8 m wave in 11 m of water.

In the case of the coast south of Rabat, the available bathymetric maps are not accurate enough (Fig. 1); however, we can infer from equation (1) that even wave heights may reach 10 m during storms (e.g. on 5 and 6 January 2008), only waves or swell of less than 6-7 m can approach the cliffs to release their full energy without breaking.

As a large number of boulders are upside-down, an increased energy is required to dislodge, lift and overturn them. Among the several cases exposed by Nott (2003), the joint bounded block

scenario seems the most appropriate to the Rabat coast, and the main force acting on the boulder is the lift force F_L , expressed by (Nott, 2003, and modified version by Noormets et al., 2004):

$$F_L = [0.5 \rho_w C_1 (bc) u^2] b / 2 \quad (2)$$

where C_1 is the lift coefficient (0.178), b and c are the length of the B-axis and the C-axis of boulder respectively, ρ_w is the mass of unit volume of water and u is flow velocity.

This force can exert a moment with a pivot point around which the boulder may rotate (Fig. 8A of Noormets et al., 2004).

Following equation (2), a 10-ton boulder would require a storm wave height of at least 18.5 m (Table 1 of Nott, 2003). Because the weight of the observed boulders is in the range 20-100 tons, storm waves can be already excluded for the coastal boulders south of Rabat, and tsunami waves with their much higher mass, velocity and energy are required.

It can also be readily seen from equation (2) that for blocks of the same size, the lift force mainly depends on the velocity of flow, which is much higher for tsunamis. Therefore, the overturning of the boulders is best explained by the lift force exerted by tsunamis.

4.2.2. Transport of blocks

The transport distance of a block on a platform can be expressed by the formula (Noormets et al., 2004, p. 57):

$$X = [T \cdot g^{1/2} \cdot ((R - E)^{1/2} - H^2)] / 5 \quad (3)$$

where X is the transport distance (m); T is the wave period (s); g is the acceleration due to gravity (m/s^2); R is the run-up elevation (m); E is the revetment crest elevation (m); and H is the bore height (m) at distance X .

Equation (3) readily shows that, for the same conditions of run-up and revetment height, the transport appears to be much longer by tsunami waves because of their longer period. For instance, for the same wave/bore heights, and taking a period of 15 s for waves and 15 min for tsunami, the distance is 60 times longer for tsunamis.

A simpler method in quantifying the energy of displacement of a boulder is calculating the "transport figure" (Scheffers, 2005, p. 39) which is given by the equation:

$$Tf = W \times D \times V \quad (4)$$

where Tf is the Transport figure; W is the weight (tons) of the block; D is the distance moved (m), and V is the vertical distance (m). The value 2,000 is regarded as to be the uppermost limit of storm wave transport energy.

At Petit Val d'Or, we found 20-ton blocks transported 150 m away from the shoreline, some of which were overturned. This gives a Tf of 3,000 without taking into account the height reached. In average, blocks of 30-60 tons are common at 10-20 m inland, so this gives Tf values of 1,500-6,000 for a +5 m elevation.

It should be noted that the value of topographic elevation is a minimum, as many blocks have been overturned, so their centre of gravity attained a higher elevation which depends on the boulder dimensions (e.g. 3 m for a 6 m large block). This leads to a large increase of the V values, and then in those of Tf .

4.3. Age of boulder dislocation

Since this study is preliminary, we have not yet collected any marine organisms at or in the boulders to absolutely date the time of their displacement out of the sea, but there are some indirect or relative age indicators for this process: nearly all boulders have been settled on a ripe bio-erosive topography, balancing on rock pinnacles in an unstable position, or leaning one against the other with touching only at 1,2 or 3 small points, e.g. in imbrication trains. Neither the surface under the boulders nor beside them shows any significant differences in weathering or erosion, and the rock pools remnants on or below the boulders are nearly exactly the same as on the rock surface aside. Pools on the boulders with inclined bottoms, however, may display the formation of a new horizontal pool bottom after deposition. The dimensions of this transformation is in the size of centimetres to 1-2 decimetres, and regarding the bio erosive process being in the order of 1-2 mm/year, the age of dislocation may be only a few hundred (100-400) years as a maximum.

4.5. Concluding remarks

Summarizing, we can state that swell waves along the Rabat coast generally break before impacting with the cliff, and when they do not break, their energy appears to be insufficient for dislodgement, overturning and long transport of boulders ≥ 10 tons. Moreover, the unstable arrangement of boulders cannot be the result storms and hurricanes as successive wave trains should have destroyed the imbricates. Therefore, there is little doubt that tsunami was the cause of the present-day pattern.

As this part of the Moroccan coastline is exposed to the Gulf of Cadiz with well known large tsunamis in former centuries, and as a tsunami wave of far more than 10 m in height (or with a run-up of more than 10 m in places) has been reported or calculated for the Lisbon tsunami of November, 1st, 1755 AD (Baptista et al., 2003; Gutscher et al. 2006), it is highly likely that this tsunami was responsible for the boulder accumulations and transport at the NW Moroccan coastlines. This is in accordance with the amount of weathering and the general aspect, that all the boulders have been dislodged and transported by the same (i.e. only one) event. Taking into account the observations along the southern Atlantic coastline of Spain near Cabo de Trafalgar (Whelan and Kelletat, 2005), where boulders of up to 100 tons have been transported on up to 300 m by the Lisbon tsunami and the Cabo de Trafalgar, 19 m high, has been overrun by the tsunami waves, this conclusion may be supported by all observations available so far.

4.6. Tsunami hazard in the Rabat coast

All the observations along the coast south of Rabat show that in the rocky zones, the boulders remain between the shoreline and the inactive cliff (Fig. 2), so their transport was restricted to the flat Oulja when the latter is present, or to the platforms in lower areas. In addition, the inactive cliff has certainly acted as a barrier against the tsunami wave and protected the eventual constructions and population uphill. On the basis of the formulas exposed by Nott (2000, 2004), which use rock density and dimension of boulders, the calculated tsunami wave heights seem to have been relatively small, in the range 3-5 m; however, the tsunami coincided with a period of high tide (+2.83 m at 14.00), thus increasing the energy.

This may have not been the case in estuaries, where the largest damage was reported by Al Kadiri from the area of Rabat and Salé (text reproduced by Elmrabet, 2005, p. 264-265). We have

no data on the estuarine formations of the Bouregreg river between Rabat and Salé for the moment, but recent surface boring of the Loukkos estuary (Aloussi, 2008), located 100 km to the north, has revealed centimetric to decametric-thick, Foraminifera-bearing, marine sands intercalated within muddy deposits at shallow depths, up to 10 kilometers inland. This attests for a probable tsunami-related invasion by seawaters. As datings are still unavailable, we cannot ascertain that these marine sands are related to the 1755 tsunami or to previous ones; however, they attest for the existence of such events in past times.

5. CONCLUSIONS

1. A survey of the rocky coastline south of Rabat (Morocco) has led to the first description of the emplacement of a large number of boulders laying upon the post-Ouljian lithified dune system along the shoreline.
2. The boulders, weighting 4-100 tons, may be single, arranged in imbricated sets, or forming clusters of hundreds. Some of the boulders have been overturned, thus showing pool apertures downwards. Transport distance is generally of some tens of meters because of the surface roughness, but some of them were found at 300 m from the shoreline.
3. All boulders have been detached from their initial position at the fractured front of the active cliff. Wave hydrodynamics and rock mechanics quantification show that dislodgement and transport of these boulders were accomplished by tsunami rather than by storm waves.
4. Although no datings were attempted, the unstable position of the boulders, the post-emplacement bio-erosion by littorinids and the absence of any erosion at the base of the boulders or in the basement rocks suggests that they were emplaced in recent times, most likely during the 1755 AD Lisbon tsunami.

The next steps of investigation should be to look for absolutely datable material to exactly date the boulder dislocation, to extend the observations along the Moroccan coastlines to the south and the north, and to try to evaluate the tsunami history of the area by coring in the sediments trapped in the swales behind the first eolianite ridge.

6. ACKNOWLEDGEMENTS

This work was initiated within the activities of the team “Marges méso-cénozoïques marocaines” at the Institut Scientifique of Rabat, and in part funded by the University Mohammed V-Agdal.

7. REFERENCES

- Akil, M. 1982. Contribution à l'étude sédimentologique des formations littorales quaternaires de la région de Rabat. Mém. Dipl. Etudes Sup., Université Mohammed V, Fac. Sci. Rabat, 139 p., 7 pl., 1 map.
- Aloussi, L. 2008. Evolution spatio-temporelle de l'estuaire du Loukkos; étude préliminaire. DESA Memoir, Fac. Sci. Rabat, 58 p. + append.
- Asebriy, L., Bucci, C., El Amrani, I.-E., Franchi, R., Guerrera, F., Martin-Martin, M., Patamia, C., Raffaelli, G., Robles Marin, P., Tejera de Leon, J. and Tentoni, L. 2007. Etude intégrée de la dégradation des monuments historique Romains et Islamiques de la ville de Rabat (Maroc): proposition de solutions durables de prévention et restauration. Science and Technology for Cultural Heritage, Pisa-Roma, 16 (1-2), 45-65.
- Baptista, M.A., Miranda, P. and Mendes Victor, L. 1992. Maximum entropy analysis of Portuguese tsunami data ; the tsunamis of 28.02.1969 and 26.05.1975. Sci. Tsunami Haz., 10(1), 9-20.
- Buforn, E., Bezzeghoud, M., Udias, A. and Pro, C. 2004. Seismic sources on the Iberia-African plate boundary and their tectonic implications. Pure Appl. Geophys., 161(3): 623-646.
- Campos, M.L. 1991 Tsunami hazard on the Spanish coasts of the Iberian peninsula. Sci. Tsunami Haz., 9(1): 83-90.
- El Alami, S.O. and Tinti, S. 1991. A preliminary evaluation of the tsunami hazards in the Moroccan coasts. Sci. Tsunami Haz., 9(1): 31-38.
- Elmrabet, T. 2005. The great earthquakes in the Maghreb region and their consequences on man and environment. Imprimerie Beni Snassene, Rabat, 428 p. (in Arabic + English summary and table).
- Gigout, M. 1957 Recherches sur le Pliocène et le Quaternaire atlantiques marocains. Trav. Inst. Sci. Chérif., Rabat, sér. Géol. et Géogr. Phys., 7, 77 p.
- Guilcher, A. and Joly, F. 1954. Recherches sur la morphologie de la côte atlantique du Maroc. Trav. Inst. Sci. Chérif., Rabat, sér. Géol. et Géogr. Phys., 2, 140 p.
- Gutscher, M.-A., Baptista, M.A. and Miranda, J.M. 2006. The Gibraltar Arc seismogenic zone (part 2): Constrains on a shallow east dipping fault plane source for the 1755 Lisbon earthquake provided by tsunami modeling and seismic intensity. Tectonophysics, 426: 153-166.
- Heinrich, Ph., Baptista, M.A. and Miranda, P. 1994. Numerical simulation of the 1969 tsunami along the Portuguese coast. Preliminary results. Sci. Tsunami Haz., 12(1): 3-23.
- Kelletat, D.H. 1997. Mediterranean coastal biogeomorphology : processes, forms and sea-level indicators. In : Transformations and evolution of the Mediterranean coastline. Bull. Inst. Océanogr., Monaco, n° sp. 18, and CIESM Sci. series, 3 : 209-226.
- Lambert, A. 1987 Animaux de la côte atlantique marocaine. Librairie Nationale, Casablanca, 207 p.

- Milliès Lacroix, A. 1974 Carte géotechnique de la région de Rabat. Notes et Mémoires du Service géologique du Maroc, n°238.
- Noormets, R., Crook, K.A.W. and Felton, E.A. 2004. Sedimentology of rocky shorelines: 3. Hydrodynamics of megaclast emplacement and transport on a shore platform, Oahu, Hawaii. *Sedim. Geol.*, 172: 41-65.
- Nott, J. 2000. Records of prehistoric tsunamis from boulder deposits. Evidence from Australia. *Sci. Tsunami Haz.*, 18, 1, 1-14.
- Nott, J. 2003. Waves, coastal boulder deposits and the importance of pre-transport setting. *Earth and Planet. Sci. Letters*, 210: 269-276.
- Saaidi, E. 1988. Géologie du Quaternaire marocain. Ed. SMER, Rabat, 439 p.
- Scheffers, A. and Kelletat, D. 2003. Tsunami relics on the coastal landscape west of Lisbon, Portugal. *Sci. Tsunami Haz.*, 23(1): 3-15.
- Scheffers, A. and Kelletat, D. 2004. Bimodal tsunami deposits – a neglected feature in paleo-tsunami research. In: Schernewski, G. and Dosch (Editors) – *Geographie der Meere und Küsten. Coastline Reports*, 1: 67-75.
- Stich, D., Mancilla, F. and Morales, J. 2005. Crust-mantle coupling in the Gulf of Cadiz (SW-Iberia). *Geophys. Res. Lett.*, 32, L13306, doi:10.1029/2005GL023098.
- Trudgill, S.T. 1987. Bioerosion of intertidal limestone, Co. Clare, Ireland. – 3: Zonation, Process and Form. *Marine Geology*, 74: 111-121.
- Whelan, F. and Kelletat, D. 2005. Boulder deposits on the southern Spanish Atlantic coast: possible evidence for the 1755 AD Lisbon tsunami. *Sci. Tsunami Haz.*, 23(3): 25-38.

TSUNAMIS OF THE ARABIAN PENINSULA A GUIDE OF HISTORIC EVENTS

Benjamin R. Jordan

*Department of Geology
Brigham Young University – Idaho
Rexburg, Idaho 83460-0510
U.S.A.
jordanb@byui.edu*

ABSTRACT

The Arabian Peninsula has been affected by tsunamis in the past. The Peninsula is bounded by the Persian Gulf on its northeast side, the Red Sea on its west side, and the Arabian Sea, the Gulf of Aden, and the Indian Ocean to its east and south. Each of these areas is very different geographically, tectonically, and bathymetrically. Only two, localized tsunamis have been recorded in the Red Sea and one, doubtful, tsunami in the Persian Gulf. Almost all of the recorded tsunamis along the Arabian Peninsula have occurred on its eastern and southern edge, some, such as the one formed by the 1945 Makran earthquake, were extremely destructive. The Indian Ocean is the most likely source area for future destructive tsunamis that would impact the Arabian Peninsula.

Keywords: Tsunami, Arabian Peninsula, Arabian Gulf, Persian Gulf, Arabian Sea, Indian Ocean

1. INTRODUCTION

The Indonesian tsunami of 26 December 2004 illustrated the horrific destruction and loss of life that a large tsunami can cause. Over 225,000 people were killed (Kerr, 2005; Geist et al., 2006) by a tsunami generated by a 9.0+ magnitude earthquake off of the northwest coast of Sumatra, where the India Plate is subducting beneath the Burma Microplate. The earthquake ruptured the seafloor surface and displaced the water column above it by several meters. The resulting wave heights near the epicenter were determined to be 32 m high. In Kenya, ~5,000 km away, wave heights were still 2-3 m high (Jaffe et al., 2005).

Minor effects from the tsunami reached the Arabian Peninsula in about 7 hours, producing mostly small waves less than 1 m in height along its coasts, except in the areas in southern Oman, especially around Salalah, where wave runup reached 3.3 m (Okal et al., 2006). Most of the Arabian Peninsula was shielded from large effects of the tsunami due to the Indian Peninsula, which took the brunt of the waves that would have otherwise inundated the peninsula's Arabian Sea/Indian Ocean coasts (Kowalik, 2005).

Another internationally well-known, large tsunami that impacted the Peninsula was the 1945 Makran tsunami. This tsunami devastated the coasts of Iran, Pakistan, and possibly Oman (Berninghausen, 1966).

The purpose of this paper is to summarize the historical records of tsunami events, both confirmed and suspected, and to discuss their impacts on the Arabian Peninsula. No specific summary has been made previously of tsunamis affecting the coasts of the Arabian Peninsula. This is partly due to the lack of and difficulty in obtaining historical records for the area and partly because until the 2004 Indonesian tsunami, little widespread interest was focused on this part of the world.

2. GEOLOGICAL BACKGROUND

The Arabian Peninsula makes up the majority of the Arabian Plate, which is moving in a northeastward direction, away from the spreading center that runs the length of the seafloor beneath the Red Sea, to where it is colliding and subducting beneath the Iran Microplate. Subduction is indicated by the seismicity of the region and the presence of the Makran-Baluchistan volcanic arc. The many earthquakes in Iran and Pakistan are a result of this collision and subduction. The volcanic arc consists of mostly Quaternary andesitic volcanoes. There are also many present-day, active, mud volcanoes in the Makran region of Pakistan (Quittmeyer and Jacob, 1979). The rate of movement is estimated to be between 4 and 5 cm/yr (Jacob and Quittmeyer, 1979; Hutchison et al., 1981; Platt et al., 1985).

The peninsula itself can be divided into three very different geographic and oceanographic regions (figure 1):

- The Persian Gulf coast
- The Indian Ocean (Gulf of Oman and Arabian Sea) coast
- The Red Sea coast

The Persian Gulf coast of the Arabian Peninsula is a flat area of dunes and sabkha, a supratidal area consisting of mud flats just above the normal high tide level in arid and semi-arid coastal regions.

Oceanographically, the Persian Gulf is a shallow sea with a maximum depth of only 60 m. The Indian Ocean coast has narrow, alluvial plains between the ocean and the steep slopes of the Omani Mountains. These mountains often extend directly to the water. This eastern coast faces the open ocean, with only a small continental shelf. The Red Sea coast extends from the Gulf of Aqaba for approximately 2,200 kms to the Gulf of Aden. Its coast is similar to that of the Indian Ocean, with alluvial plains extending from the mountains that form the Arabian Shield complex. The Red Sea has maximum depths up to ~2850 m, but 65% of it is less than 50 m in depth. It is also very narrow, ranging between 306 to 355 km at its maximum (SGS, 2006).

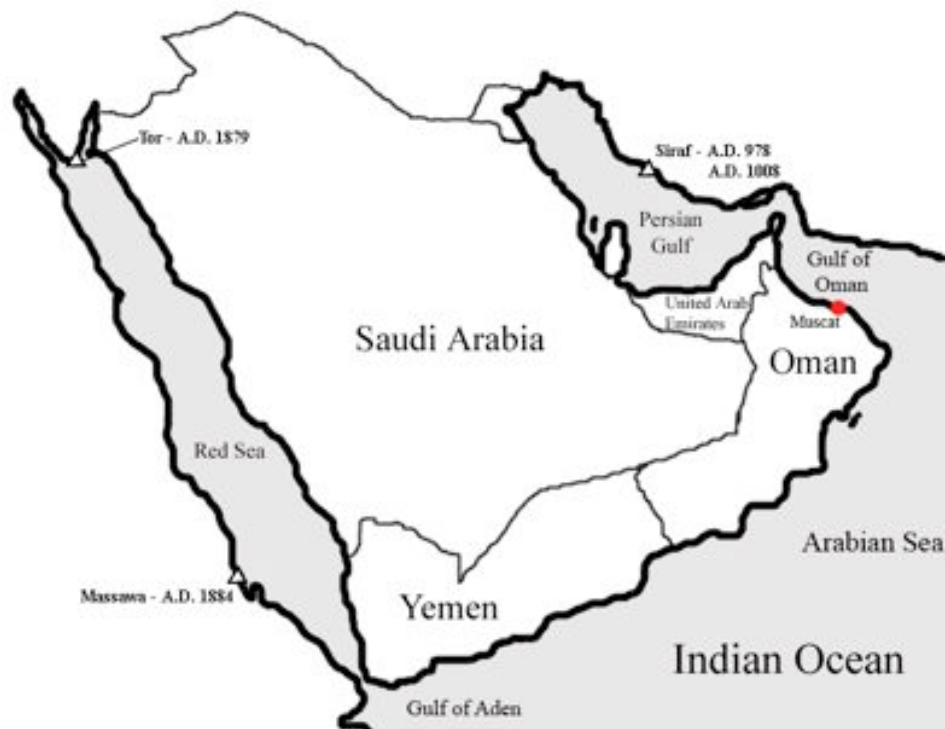


Figure 1: The Arabian Peninsula with its three coastlines.

3. TSUNAMI GENERATION

The largest sources of tsunamis in the Eastern Hemisphere are along the Sumatra subduction zone on the eastern side of the Indian Ocean (Jaffe, 2005). Since tsunami height is related to water depth, the deeper the water the larger the potential size of a tsunami. It is believed that the very large size of the Indonesian tsunami was due not only to the magnitude of the earthquake and seafloor rupture, but also because the seafloor displacement took place near a deep sea trench, in very deep water (Geist et al., 2006). The depth of the Indian Ocean then allowed the wave to travel great distances without losing much energy.

Large storms and cyclones occur in the region, but not frequently. The flooding and damage caused by their storm surges sometimes has been confused with that of tsunamis. On 4-5 June 1890, a large cyclone generated a destructive storm surge that swamped Muscat in Oman and killed several hundred people. This event was followed by another large storm in June of 1898. A similar storm is thought to have struck in same area in 863 A.D. (Lorimer, 1815). There was confusion, particularly in ancient times, between what would be considered true tsunamis and large storm-generated waves. This has made it difficult to properly determine historical tsunami events. In this paper, all known and suspected events are presented and discussed.

3.1 Methods

The historical data of tsunamis relative to the Arabian Peninsula presented in this study is based on a survey of past records, a review of the scientific literature and on media reports. All the information from the scientific literature was taken from studies related to the seismicity of the region and past earthquakes. The best resources summarizing historical seismic events in the region are the catalogs prepared by Ambraseys and Melville (1982) and by Ambraseys et al. (1994). Although these studies focus on earthquakes, they note also a number of tsunami events. Also examined for additional tsunami information were other historical records held at the Zayed Center for Culture and Heritage in the UAE. Although many recent publications already contain much of the tsunami information as for example in Rastogi and Jaiswal (2006), the significance of this paper is that it brings together, to the extent possible, a compilation of information specifically related to the Arabian Peninsula region.

3.2 Tsunami Events

The following are recorded tsunami events that have impacted the Arabian Peninsula. They are organized by geographic and oceanographic regions and are summarized in Table 1:

Persian Gulf.

978 – Siraf, Iran. On 17 June 978 A.D. the port town of Siraf, Iran, located in the Bushehr Province along the northeastern Persian Gulf coast (figure 1) - near the present port of Taheri - was struck by an earthquake which killed about 100 people. According to historical records the land shook for seven days and that some of the buildings of the town fell into the sea (McEvelly and Razini, 1973). Although there is no mention that this event generated a specific tsunami, forty years later in 1008 A.D. another earthquake (see event below) reportedly did.

1008 – Siraf, Iran. In the spring of 1008 A.D. an earthquake occurred in this region and reportedly generated waves that sunk a number of ships, with the loss of all hands on board. Also, McEvelly and Razani (1973) indicate that many people were killed when “the sea inundated the land”. Although, Ambraseys and Melville (1982) concur on the loss of several ships, they state that there is no evidence of waves inundating the land. According to them, at least one other source refers to the sinking of the ships but did not associate the waves with the earthquake. Other records show that high winds affected the region during this same time period, thus the reported flooding and destruction of ships could have been caused by storm surge. Also, there is no definitive record that waves were generated when the more destructive 978 A.D. earthquake occurred in the same location (McEvelly and Razani, 1973; Ambraseys and Melville, 1982, p. 39, 107, 176). It is possible that the reported waves may have been generated by an earthquake-triggered coastal landslide – although the historical records do not indicate that one occurred in conjunction with this particular event, or any other earthquake in the Persian Gulf region. Given this uncertainties, it is difficult to evaluate what possible effects from such a tsunami may have had along the Arabian coast or to estimate its maximum height and runup. Given the fact that wave activity was only reported in the earthquake’s epicentral region, the implication is that this event was localized and if a tsunami was indeed generated, its energy was quickly attenuated, given the shallowness of the Gulf.

The Red Sea

1879 – Tor (present-day El Tor), Egypt. On 11 July 1879, three moderate earthquake shocks were felt in upper Egypt. Although the exact locations of these earthquakes are not known, it was reported that a tsunami flooded the village of Tor on the Sinai peninsula in the Gulf of Suez (Ambraseys et al., 1994) (figure 1). A landslide is a possible source for this tsunami, but there is no such documentation in the historical records.

1884 – Massawa (present-day Mitsiwa), Eritrea. On 20 July 1884, an earthquake occurred at sea offshore from Massawa (figure 1). Reportedly, sea waves built up in the Massawa harbor, mostly between the localities known as Taulud and Edaga Barai. The waves swept over a causeway and ships in the harbor were seen swaying violently. Multiple flooding from the sea over land left dead fish onshore (Ambraseys et al., 1994).

Indian Ocean/Arabian Sea

325 B.C. – Port of Alexander (Near present-day Karachi, Pakistan). Some reports have dated this event to 326 B.C., but 325 B.C. may be more accurate. A large wave believed to be a tsunami, damaged the Macedonian fleet of

Alexander the Great while at anchor east of the present-day Karachi. The damaging waves probably originated in the same source region as the destructive 1945 Makran tsunami. Its effects on the Arabian Peninsula would likely have been similar to those in 1945 event. The description of Diodorus Siculus (c. 90 BC - c. 30 BC) of a tsunami that struck the Macedonian Fleet has been credited by some to be describing this event (Oldfather, 1989), but is more likely describing an event that occurred elsewhere in Alexander's Empire
(see <http://www.drgeorgepc.com/Tsunami325BCIndiaAlexander.html>).

1524 - Dabul, India. In 1524 the arrival of Vasco de Gama's fleet on the western coast of India also coincided with a large "sea quake" and tsunami (Bendick and Bilham, 1999; PMD, 2005). It is not known if this event occurred only locally or regionally. Since an earthquake was not reported onshore, this may indicate that the tsunami was generated at a more distant location. The Makran region of Pakistan has been suggested as a possible source (Bilham, 2004). If that is the case, then the eastern coasts of the Arabian Peninsula would have been impacted by the tsunami as well.

1819 – Rann of Kachchh, India. A large (7-8 M_s) earthquake occurred on 16 June 1819, in the Kutch region on the western coast of India. It has been suggested that the quake was caused by a near-surface reverse fault (Bilham, 1999). It is estimated that 7-9 m of crustal displacement occurred (Quittmeyer and Jacob, 1979), which generated a destructive tsunami. The Indian town of Sindri was submerged by an intruding flood that occurred as the coastal land sank an estimated 4-5 m (Berninghausen, 1966; Quittmeyer and Jacob, 1979; Bilham, 1999). In addition, a dam was formed, backing up a distributary of the Indus River (Bilham, 1999). Just as with the previous event, the most likely area of the Arabian Peninsula that would have been affected by this tsunami would have been the southern and eastern coasts. The tsunami travel time would have been approximately 4 hours (Bhaskaran et al., 2005).

1845 – Kutch, India. Following an earthquake, eyewitnesses described a large wave from the sea that caused the mouth of the Indus River to overflow the surrounding land. Unfortunately, other than the general region of the Indus, other geographical names used in the description cannot be located (Berninghausen, 1966). In the event that this was a true tsunami, it is highly unlikely that it had a any significant effect on the Arabian Peninsula.

1851 – Makran, Pakistan. The Makran coast of Pakistan lies on the southern edge of Pakistan, to the northeast of Oman. Okal et al. (2006) mention a seismic event that may have occurred in 1851 off Makran, west of the 1945

tsunamigenic earthquake but with no details as to whether a tsunami was generated. However, given the proximity of this event to the 1945 tsunami source, it is possible that a tsunami was generated and that the region has the potential to generate tsunamis that could impact the Arabian Peninsula.

1883 – Krakatau, Indonesia. The eruption of Krakatau Volcano near the Sunda Strait of Indonesia on 28 August 1883 produced a destructive tsunami that devastated villages and towns and killed nearly 36,000 people in the immediate area. Sea level oscillations were observed worldwide and recorded by tide gauges at distant locations. The tsunami was generated by a combination of caldera and slope collapse, pyroclastic flows, subsidence and final explosion and collapse (Berninghausen, 1966; Pararas-Carayannis, 2003; Winchester, S., 2003). Once outside the Sunda Strait the waves attenuated quickly in height. In Karachi, Pakistan the maximum wave was measured at 37 cm in height. It took an estimated 12 hours travel time for the wave to reach the Gulf of Aden on the southern end of the Arabian Peninsula, where the tide gauge registered a tsunami wave that was 13 cm in height (Berninghausen, 1966; Pararas-Carayannis, 2003). The eastern portion of the peninsula would have felt the affects of the wave in about 9.5 hours (Bhaskaran et al., 2005) with somewhat greater wave-heights, but no other Arabian records could be found for the event.

1945 – Makran, Pakistan. At 03:26 IST (Indian Standard Time) on 28 November 1945 an 8.1 magnitude earthquake was generated in the northern Arabian Sea off the Makran coast (Berninghausen, 1966; Quittmeyer and Jacob, 1979; Ambraseys and Melville, 1982). The earthquake was felt in Karachi, Pakistan, where ground motions (figure 2) lasted approximately 30 seconds, stopping the clock in the Karachi Municipality Building and interrupting the communication cable link between Karachi and Muscat, Oman (Omar, 2005). Ground motions were felt as far away as Calcutta, on the eastern side of the Indian subcontinent (Ambraseys and Melville, 1982; Byrne et al., 1992; Pacheco and Sykes, 1992; Pararas-Carayannis, 2006; Omar, 2005).

The epicenter is estimated to have been at 24.20 N, 62.60 E, about 408 km SSW of Karachi and 465 km NNE of Muscat, Oman. The quake caused extensive damage throughout the region. Subsequent eruptions of mud volcanoes in the Balochistan region of Pakistan, formed four small islands.

The damage from the earthquake was great, but the greatest destruction to the region was caused by the tsunami that was generated. Tsunami waves "swept the whole of the Arabian Sea coast" (Berninghausen, 1966, p. 73). It is estimated that 4,000 people were killed. The fishing village of Khudi, Pakistan and its entire population, 48 km west of Karachi, was swept away. The trading towns of Pasni and Ormara, Pakistan, located 100 km away from the

epicenter, were flooded by a ~15 m high wall of water (Murty and Bapat, 1999; PTI, 2004; Omar, 2005). At least three waves (05:30, 07:00, 08:15 IST), over 2 m high, reached Karachi 408 km away, as well as Bombay, which was 1,200 km away (Ambraseys and Melville, 1982; Omar, 2005). In Karachi the waves persisted for so long that significant harbor damage and loss of life occurred. During the strong drawdown of the water preceding the tsunami in Keti Bandar of the Indus Delta "low-lying hills collapsed and spread out, totally destroying a number of fishing villages" (Ambraseys and Melville, 1982, p. 90). This tsunami reached eastward as far as Karwar, India, 1,600 km away (IST, 2004).

The tsunami was recorded along the coasts of Iran and in Muscat, Oman, which is 580 km from the source, and where there was considerable damage and loss of life (ASC, 2003; Pararas-Carayannis, 2006). In addition, a boat traveling from Muscat to Karachi was lost (Ambraseys and Melville, 1982, p. 90, 193).

The tsunami travel time to the Arabian Peninsula would have been less than an hour (Bhaskaran et al., 2005). It is assumed that if the tsunami affected Muscat as well as coastal cities in Iran, more than likely it affected also the United Arab Emirates (UAE) and Indian Ocean coastal communities, such as Khorfakkan and Fujairah. Persistent seismic activity in the Northern Arabian Sea since 1945, implies that the potential for other large earthquakes may exist for this region (Quittmeyer, 1979).

Although there are also no direct records of this tsunami in the Arabian Gulf, at Julfar, the forerunner of Ras al-Khaimah, UAE, there was a large sandbar that ships use to have to transport goods over. It was noted that sometime before 1964 this bar was breached by a "tidal wave", which formed a direct channel from the open sea to the harbor. Ambraseys and Melville (1982, p. 193) have suggested that this wave was associated with the 1945 Makran tsunami.

1983 – Chagos Archipelago. On 30 November 1983 the Chagos Archipelago and the island of Diego Garcia were struck by a 6.6 M earthquake. The epicenter was at 6.85 S, 72.11 E. Locally, the quake produced a tsunami with maximum height of 1.5 m. By the time this tsunami reached Seychelles to the west, 1,700 km away, it had attenuated to 40 cm in height (USGS, 2002). Although this tsunami had no obvious impact on the Arabian Peninsula, the location of the Chagos Archipelago in the middle of the Indian Ocean indicates that a larger earthquake from this region has the potential to produce a tsunami that can adversely impact affect other Indian Ocean coasts, including those of the Arabian Peninsula.

2004 – Aceh, Indonesia. As mentioned previously, the 26 December 2004 earthquake generated a large tsunami that affected the entire Indian Ocean basin. It did not greatly impact the Arabian Peninsula, but small waves

ranging from 3 to 30 cm in height occurred along the northern Arabian Peninsula coasts, adjacent to the Gulf of Oman (Kowalik et al., 2005). However, further south, from Shannah, Oman to Dhalkut, Oman, the wave runup heights varied between 0.8 m to 3.3 m (Okal et al, 2006). At the port of Salalah, large eddies formed. One freighter actually broke loose from its mooring and drifted for several hours (Okal et al. 2006). Local fisherman in Rakhyut (just north of Dhalkut), near the Oman-Yemen border, where the tsunami runup was 2.6 m (Okal et al., 2006), noticed a discoloration of the water and unusual surface wave behavior (local fishermen-personal communication).

Table 1. Summary of tsunamis related to the Arabian Peninsula

Date	Source Location	Description
Persian Gulf		
A.D. 978, 17 June	Siraf, Iran	Large earthquake, but not followed by a tsunami
A.D. 1008, Spring	Siraf, Iran	Large earthquake with reports of ships sinking, but ships likely sank due to a concurrent storm, not tsunami
Red Sea		
A.D. 1879, 11 July	Tor (present-day El Tor), Egypt	Moderate earthquakes were felt in upper Egypt, village of Tor inundated by tsunami
A.D. 1884, 20 July	Massawa (present-day Mitsiwa), Eritrea	Offshore earthquake occurred, sea waves built up in harbor and swept over causeway.
Indian Ocean/Arabian Sea		
326 B.C., November	Southern Pakistan	Tsunami sank Macedonian ships - this event probably did not occur.
A.D. 1524	Dabul, India	Tsunami occurred, but no earthquake was felt - this event was probably local and did not affect Arabia.
A.D. 1819, 16 June	Gujrat, India	Large earthquake in western India generated a large tsunami - the wave would have arrived in Arabia in about 4 hours, but there is no record of effects in the Arabian Peninsula.
A.D. 1845	Kutch, India	An earthquake was followed by a small tsunami - this event was probably too small to have affected the Arabian Peninsula.
A.D. 1851	Makran, Pakistan	An earthquake occurred off of the Makran coast with an epicenter west of the better known 1945 earthquake epicenter and tsunami
A.D. 1883, 8 August	Krakatau, Indonesia	The eruption of Krakatau volcano generated a large tsunami, which was measured worldwide. A station located in the Gulf of Aden measured a small tsunami 13 cm in height. No other records are apparent for Arabia.
A.D. 1945, 28 November	Makran, Pakistan	A large earthquake off of the southern coast of Pakistan generated a large tsunami that devastated the region, killing more than 4,000 people. This wave may have also swept into the Persian Gulf and washed out a large sandbar at Ras al-Khaimah, UAE.
A.D. 1983, 30 November	Chagos Archipelago	An earthquake at the Island of Diego Garcia produced a small tsunami (1.5 m high) - its small size did not produce any recordable impacts on the Arabian Peninsula, but future events from the same location could.
A.D. 2004, 26 December	Aceh, Indonesia	An extremely large earthquake generated a 10-15 m high tsunami that killed over 225,000 people. It had minor impacts along the southern Arabian coast.

4. DISCUSSION

Similarly, there appears to be very little tsunami threat in the Red Sea. In spite of the fact that the Red Sea is a seismically active region, only the two small tsunami events described here have been documented for the Red Sea. Given that the sea is a tectonically divergent environment, the likelihood of very large, tsunami-generating, earthquakes is relatively small.

It is obvious from the historical summary that the greatest tsunami threat facing the Arabian Peninsula comes from sources in the Indian Ocean. The Sunda Arc, presents the major tsunami hazard in the Indian Ocean, due to its earthquakes and volcanic eruptions, however is not likely a major source of danger to the Arabian Peninsula given the buffering effect of the Indian Subcontinent. Instead, the region of greatest danger is that of the Northern Arabian Sea. The 1524 and the 1945 events had their sources in the Arabian Sea and both generated significant and destructive tsunamis. Okal and Synolakis (2008) provide a more detailed explanation of the Indian Ocean tsunami hazards, including a detailed discussion of seismic sources near the Makran coast of Pakistan that generated the 1945 event.

Within the Persian Gulf it is rather unlikely for large tsunamis to form. Given that the Gulf is shallow, does not have coastlines prone to landslides, and is without volcanoes, the likelihood for tsunamis is relatively small. Although the Gulf is a tectonically active region, most of the earthquakes take place inland, away from the coasts. This is reflected in the historical record. With the exception of the 1008 A.D event, which is not conclusive – as it may have been the result of storm surge - none of the other historical or more recent submarine or coastal earthquakes have generated tsunamis of any significance. Table 2 lists the known large earthquakes that have occurred within the Persian Gulf and its coasts. In every case, except for the questionable 1008 A.D. event, no tsunamis resulted. The possibility of the 1945 event breaching the bar at Julfar notwithstanding, the coasts of the Persian Gulf are protected from tsunamis generated in the Indian Ocean by the protective buffer of Musandam Peninsula in the Strait of Hormuz.

5. CONCLUSIONS

There are only a few recorded tsunami events that have impacted the Arabian Peninsula. The most destructive ones had their origin in the Indian Ocean. There are indications that the one tsunami event in the Persian Gulf may not have even been a tsunami at all and the two events in the Red Sea were small and localized. Given the shallow nature of the Persian Gulf and the lack of confirmable tsunami events in the past, it can be concluded that the risk of tsunamis in the Arabian side of the Persian Gulf is very small. The same is true for the Red Sea since, although active, does not have the very large seismic events that result in a convergent environment. On the other hand the Arabian Sea and Indian Ocean, which borders the eastern coasts of Arabia are large potential source areas for tsunamis that could seriously affect its coasts.

6. ACKNOWLEDGMENTS

Dr. James Fletcher of UAEU should be given the credit for asking me the initial questions that led to this paper. This work could also not have been completed without the help of individuals at the Zayed Centre for Heritage and History in Al Ain, UAE, especially Hamden Rashid, who allowed me free access to the center's documents. I would also like to especially thank Tad S. Murty at the University of Ottawa, Canada, Shishir K. Dube of the Indian Institute of Technology, Kharagpur, India, and Mohammad Mokhtari of the International Institute of Earthquake Engineering and Seismology in Iran, for their encouragement and generosity in sharing information. I also appreciate a review done by Ruth S. Ludwin of the University of Washington. Members of the Tsunami Reconnaissance Team, especially Walter Hays, Paul Grundy, and Nicholas Ambraseys helped direct me to possible source material.

7. REFERENCES

- Ambraseys, N. N., and Melville, C. P., 1982, A History of Persian Earthquakes, Cambridge University Press, New York, New York, 219 pages.
- Ambraseys, N. N., Melville, C. P., and Adams, R. D., 1994, The Seismicity of Egypt, Arabia and the Red Sea, Cambridge University Press, New York, New York, 181 pages.
- ASC, 2003. 1945 – Off the Makran Coast (Balochistan), Pakistan, Mw 8.0. Amateur Seismic Center, <http://asc-india.org/gq/mekran.htm>.
- Bendick, R., and Bilham, R., 1999, Search for buckling of the southwest Indian coast related to Himalayan collision, *In* Macfarlane, A., Sorkhabi, R., and Quade, J. (Eds.), 1999, Himalaya and Tibet: mountain roots to mountain tops, *Geological Society of America Special Paper* 328, p. 313-323.
- Berninghausen, W. H., 1966, Tsunamis and seismic seiches reported from regions adjacent to the Indian Ocean, *Bulletin of the Seismological Society of America*, v. 56. p. 69-74.
- Bhaskaran, P. K., Dube, S. K., Murty, T. S., Gangopadhyay, A., Chaudhuri, and Rao, A. D., 2005, Tsunami Travel Time Atlas for the Indian Ocean, Indian Institute of Technology, Kharagpur, India, 286 pages with CD.
- Bilham, R., 1999, Slip parameters for the Rann of Kachchh, India, 16 June 1819 earthquake quantified from contemporary accounts, in Stewart, I. S. & Vita-Finzi, C. (Eds) Coastal Tectonics. *Geological Society London*, v. 146, p. 295-318.
- Bilham, R., 2004, Earthquakes in India and the Himalaya: tectonics, geodesy and history, *Annals of Geophysics*, v. 47, p. 839-858.
- Byrne, D. E., Sykes, L. R., and Davis, D. M., 1992, Great thrust earthquakes and aseismic slip along the plate boundary of the Makran subduction zone, *Journal of Geophysical Research*, v. 97, p. 449-478.
- Geist, E. L., Titov, V. V., and Synolakis, C. E., 2006, Tsunami: wave of change, *Scientific American*, January 2006, p. 56-63.
- Hutchison, I., Loudon, K. E., White, R. S., and von Herzen, R. P., 1981, Heat flow and age of the Gulf of Oman, *Earth and Planetary Science Letters*, v. 56, p. 252-262.
- IST, 2004, Tsunami had Hit India in 1945, Reveals Scientist, India News.Net, 28 December, 2004.

- Jackson, J. (Ed.), 1997, Glossary of Geology (4th Edition), American Geological Institute, Alexandria, Virginia, 769 pages.
- Jacob, K. H., and Quittmeyer, R. L., 1979, The Makran Region of Pakistan and Iran: trench-arc system with active plate subduction. *In* Farah, A., and DeJong, K. A. (eds.), 1979, *Geodynamics of Pakistan*, Geological Survey of Pakistan, Quetta, p. 305-317.
- Jaffe, B., Geist, E., and Gibbons, H., 2005, Indian Ocean earthquake triggers deadly tsunami, *Sound Waves*, v. FY 2005, n. 68, p. 1-3.
- Kerr, R.A., 2005. Failure to gauge the quake crippled the warning effort. *Science*, 307(5707), 201.
- Kowalik, Z., Knight, W., Logan, T., and Whitmore, P., 2005, Numerical modeling of the global tsunami: Indonesian tsunami of 26 December 2004, *Science of Tsunami Hazards*, v. 23, n. 1, p. 40-56.
- Lisitzin, E. (1974), *Sea Level Changes*, Elsevier Oceanographic Series, No.8, New York, 273 pages.
- Lorimer, J. G., 1815, *Gazetteer of the Persian Gulf, 'Oman, and Central Arabia*, Part II, p. 2205-2219.
- McEvelly, T. V., and Razani, R., 1973, The Qir, Iran earthquake of April 10, 1972. *Bulletin of the Seismological Society of America*, v. 63, p. 339-354.
- Murty, T.S., and Bapat, A., 1999. Tsunamis on the Coast Lines of India. 1999 Tsunami Symposium Program and Abstracts, URL: <http://www1.tpgi.com.au/users/tps-seti/tsym.html#murt>.
- Oldfather, C. H. (trans.), 1989, Diodorus Siculus. Diodorus of Sicily in Twelve Volumes with an English Translation by C. H. Oldfather. Vol. 4-8. Cambridge, Mass.: Harvard University Press; London: William Heinemann, Ltd.
- Okal, E. A., Fritz, H. M., Raad, P. E., Synolakis, C., Al-Shijbi, Y., and Al-Saifi, M., 2006, Oman field survey after the December 2004 Indian Ocean Tsunami, *Earthquake Spectra*, v. 22, n. S3, p. S203-S218.
- Okal, E. A. and Synolakis, C., 2008, Far-field tsunami hazard from mega-thrust earthquakes in the Indian Ocean, *Geophysical Journal International*, v. 172, p. 995-1015.
- Omar, K., 2005. Over 4,000 People were killed when Tsunami hit Balochistan Coast. The News International, Pakistan, 9 April 2005.
Science of Tsunami Hazards, Vol. 27, No. 1, page 43 (2008)

- Pacheco, J.F., and Sykes, L.R., 1992. Seismic Moment Catalog of Large Shallow Earthquakes, 1900-1989. Bulletin of the Seismological Society of America, 82, 1306-1349.
- Pararas-Carayannis, G., 2003, Near and far-field effects of tsunamis generated by the paroxysmal eruptions, explosions, caldera collapses, massive slope failures of the Krakatau Volcano in Indonesia on August 26-27, 1883, *Science of Tsunami Hazards*, v. 21, n. 4., p. 191-201.
- Pararas-Carayannis, G., 2006. The Potential of Tsunami Generation Along the Makran Subduction Zone in the Northern Arabian Sea - Case Study: The Earthquake of November 28, 1945, *Science of Tsunami Hazards*, Vol. 24, No. 5, pages 358-384 (2006)
- Platt, J. P., Leggett, J. K., Young, J., Raza, H., and Alam, S., 1985, Large-scale sediment underplating in the Makran accretionary prism, southwest Pakistan, *Geology*, v. 13, p. 507-511.
- PMD, 2005, History of Tsunamis in Pakistan/Arabian Sea. PAKISTAN METEOROLOGICAL DEPARTMENT, January 2005.
- PTI, 2004. 1945 Tsunami Wiped off Trading Town, Hit Mumbai. The Press Trust of India, 28 December 2004.
- Quittmeyer, R. C., 1979, Seismicity variations in the Makran Region of Pakistan and Iran: relation to the great earthquakes, *Pageoph*, v. 117, p. 1212-1228.
- Quittmeyer, R. C., and Jacob, K. H., 1979, Historical and modern seismicity of Pakistan, Afghanistan, northwestern India, and southeastern Iran. *Bulletin of the Seismological Society of America*, v. 69, p. 773-823.
- Rastogi, B. K., and Jaiswal, R. K., 2006, A catalog of tsunamis in the Indian Ocean, *Science of Tsunami Hazards*, v. 25, p. 128-143.
- SGS, 2006, Saudi Geological Survey, URL:
http://www.sgs.org.sa/print_view.cfm?id=0&sec=221&page=
- USGS, 2002, Significant Earthquakes of the World for 1983, URL:
http://neic.usgs.gov/neis/eqlists/sig_1983.html
- Winchester, Simon (2003). *Krakatoa: The Day the World Exploded, 27 August 1883*, HarperCollins, New York, New York, 432 pages.

Table. 2: Recorded large earthquakes in the Persian Gulf

Year (A.D.)	Date	Location	Tsunami	Comments
1008	Spring	Siraf, Iran	large waves sank ships	It is not clear if this was a tsunami or storm surge
1426	November	near Bahrain	none recorded	
~1832		Hufuf, Saudi Arabia	none recorded	
1858	13 June	Bushire, Iran	none recorded	
1884	19 May	Qishm, Iran (island)	none recorded	Felt at Ra's al- Khaima
2005	27 November	Qeshm, Iran (island)	none recorded	Felt in Dubai and Sharjah, UAE

Taken from Ambraseys et. al. (1994) and newswire (AP) services



Figure 2. "Frozen Earthwaves" – photograph of an island off of the Makran, Pakistan coast during the 1945 Makran earthquake. The picture from the Karl V. Steinbrugge collection at the University of California-Berkeley. Image courtesy of the National Information Service for Earthquake Engineering (nisee), University of California-Berkeley. Slide number S821.

**A STUDY OF GROUNDWATER QUALITY IN TSUNAMI
AFFECTED AREAS OF SIRKAZHI TALUK, NAGAPATTINAM
DISTRICT, TAMILNADU, INDIA**

N. Ravisankar and S. Poongothai

Department of Civil Engineering
Faculty of Engineering and Technology
Annamalai University, Annamalainagar-608002

ABSTRACT

The 26, December 2004 tsunami had major impact on the quality of groundwater along the south-east coast of India, but especially in the tsunami-affected areas of the Nagapattinam district of Tamilnadu. Major pollution resulted primarily from increases in the salinity of groundwater. The post-tsunami water quality posed problems to general health and contributed significantly to agricultural and environmental degradation in the Sirkazhi taluk and Nagapattinam districts. The adverse impact was particularly significant in the areas of Pazaiyar, Madavaimedu, Thirumullaivasal, Thoduvai, Koozaiyar, Puthupattinam, Kizhamoovarkarai, Pombhukar and Vanagiri. The present study assesses the source, degree, extent and nature of groundwater contamination in the Sirkazhi coastal region. Samples of groundwater were collected from 11 wells in this area and analyzed chemically to determine the extent of contamination. The results showed significant variations in water quality parameters in the study area and helped understand the longer-term adverse impacts that tsunami inundation can have upon groundwater resources.

Keywords: Tsunami, Coastal areas, Groundwater quality.

Science of Tsunami Hazards, Vol. 27, No. 1, page 47 (2008)

1. INTRODUCTION

The 26, December 2004 tsunami flooded large coastal areas of the Nagapattinam district in Tamilnadu, destroyed vegetation along the coastal belt, and caused significant shoreline erosion. Also, the tsunami inundation affected greatly the groundwater supply. Since the quality of public health for the people in this coastal region depends to a great extent on the quality of drinking water, it was imperative to determine the effects of the tsunami.

2. STUDY AREA

The study area is the Sirkazhi taluk coastal region, in the southern Tamilnadu State located in the east coastal region of the Bay of Bengal between $11^{\circ} 6' 00''$ N and $11^{\circ} 27' 00''$ N and $79^{\circ} 36' 00''$ E and $79^{\circ} 54' 00''$ E. Figure 1 shows the study area and sample locations.



Figure. 1: Study area with sample locations (After Tsunami)

3. MATERIALS AND METHODS

Groundwater samples were collected during the month of January 2005 (beginning 13 days after the impact of the tsunami) from 11 wells in the study area for detailed quality analysis (figure 1). The names of the sampling locations at Pazhyar (two sample locations), Dharkaz, Madavaimedu, Puthupattinam, Puthupattinam (two sample locations), Kotiyamedu, Thandavankulam, Thirumullaivasal, Thoduvai and Koozhaiyar.

The samples were analyzed in the laboratory for pH, electrical conductivity, chlorides, sodium, hardness, dissolved oxygen, percentage salinity and turbidity. The concentrations of the various chemical parameters are expressed in mg/liter. The results of the water quality parameters for the 11 samples location areas are shown in Table 1 and compared with standards of the World Health Organization (WHO) and the Bureau of Indian Standards (BIS).

4. RESULTS AND DISCUSSION

The findings are summarized in Table 1. Sample parameter variations are presented in Figure 2(a) to 2(h). The results show that the pH, one of the primary parameters in the assessment of water quality was well within the prescribed norms in all the locations and in all the samples. It ranged from 6.5 to 7.07, and it was neither sharply acidic nor alkaline in nature. Hardness is defined as the sum of the polyvalent cations present in the water, notably calcium and magnesium. In the present study, the hardness varied between 264 – 2000 mg/lit.

WHO has fixed 150 mg/lit as the standard value while BSI has fixed 300 mg/lit as the limit. Puthupattinam 1, Puthupattinam 2 and Thandavankulam are the places where hardness values were below 300 mg/lit. All other remaining places had high values in hardness. According to Durfor Beckers, water with 180 mg/lit or more hardness is very hard. Almost all the samples exceeded 180 mg/lit. Excess hardness may cause health hazards like kidney stones and other ailments (Jain 1996).

Table 1: Groundwater quality parameters of study area.

Sl No	Name of the Sampling Place	Date of Sampling	pH	EC mhos	Chlorides [mg/lit]	Na [mg/lit]	Hardness [mg/lit]	Salinity [%]	Turbidity [NTU]	DO [mg/lit]
1	Pazhyar 1	09.01.2005	6.71	10.10	3058	1300	1900	8	Nil	6.7
2	Pazhyar 2	09.01.2005	6.72	11.86	2321	1310	2000	10	Nil	6.2
3	Dharkaz	09.01.2005	6.77	2.65	1547	610	652	3	Nil	7.5
4	Madavamedu	09.01.2005	6.58	4.24	1400	840	888	3	43	7.3
5	Pudupatinam 1	09.01.2005	7.07	0.541	160	70	264	0	Nil	7.3
6	Pudupatinam 2	09.01.2005	6.69	0.781	140	180	292	0	15	7.5
7	Kotiyamedu	09.01.2005	7.03	5.45	1760	780	980	4	Nil	7.7
8	Thandavankulam	09.01.2005	6.77	0.622	160	70	272	0	Nil	7.7
9	Tirumullaivasal	09.01.2005	6.5	1.236	230	240	328	2	Nil	7
10	Thoduvai	09.01.2005	6.64	4.72	1360	590	1040	4	Nil	7.4
11	Koozhaiyar	09.01.2005	6.7	4.01	1300	560	648	3	9	7.8

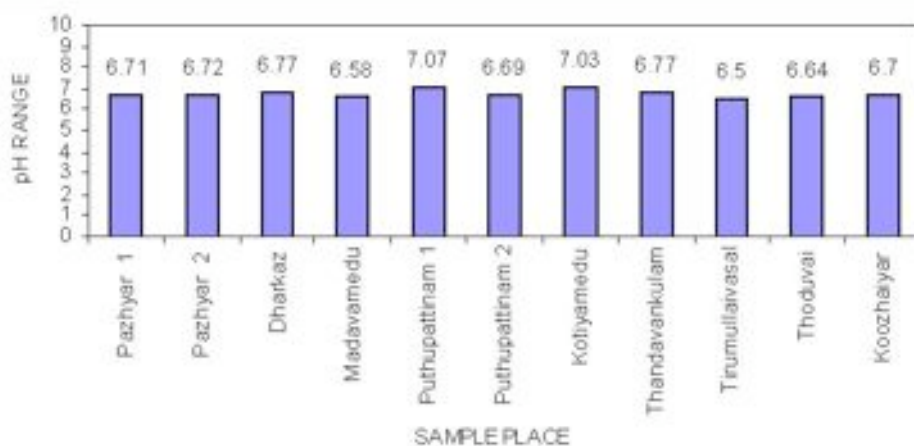


Figure. 2 (a): Water quality parameter (pH)

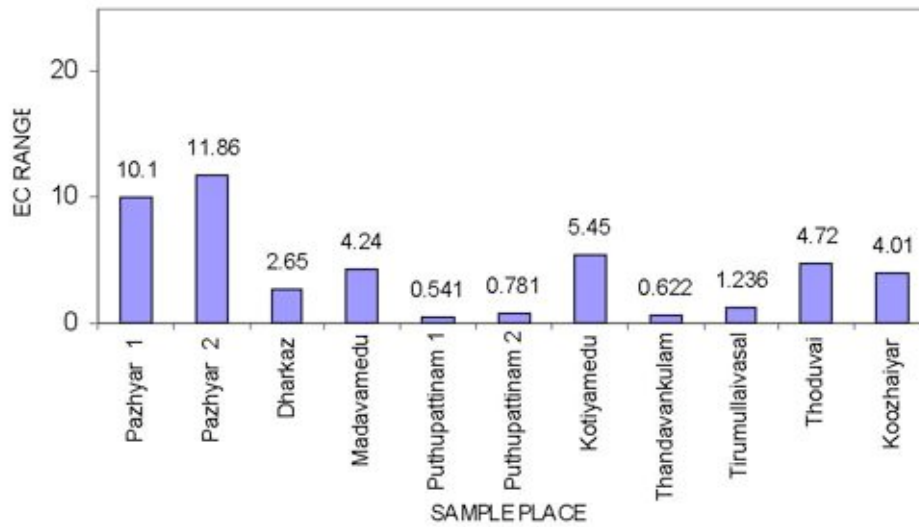


Figure. 2 (b): Water quality parameter (EC)

Natural water contains low chloride. Higher concentration of chloride in water is often found in conjunction with higher sodium concentration. WHO and BIS have prescribed 250 mg/lit as the maximum permissible value. If the chlorine value exceeds 300 mg/lit and the presence of a major cation is sodium, then the water becomes salty. The present study shows that the samples in Puthupattinam 1, Puthupattinam 2, Thandavankulam and Thirumullaivasal were well within the BIS limit while the others are higher than the norms.

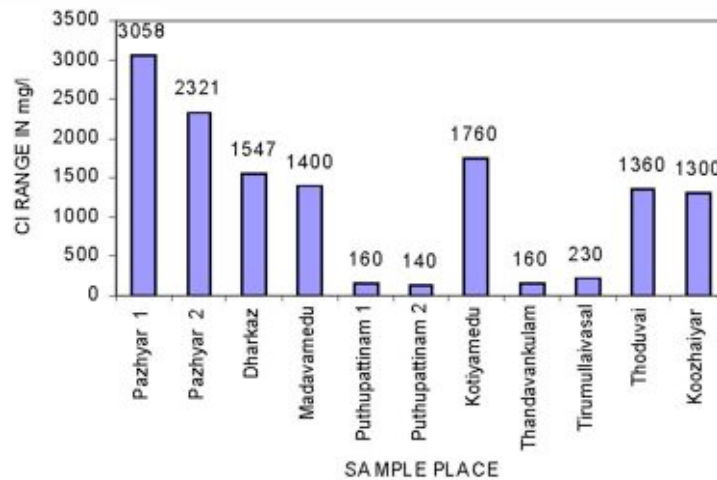


Figure. 2 (c): Water quality parameter (Cl)

Dissolved oxygen (DO), a vital parameter in the stability of the aquatic eco-system, was within the prescribed norms (6.2 – 7.8 mg/lit). The electrical conductivity (EC) is the parameter, which influences agricultural crops. The present study shows that the EC ranged from 0.571mhos to 11.16 mhos. Puthupattinam 1, Puthupattinam 2, and Thandavankulam showed lesser concentrations but other location had high concentrations. Sodium concentration is an important factor in classifying irrigation water. High level of sodium inhibits soil permeability.

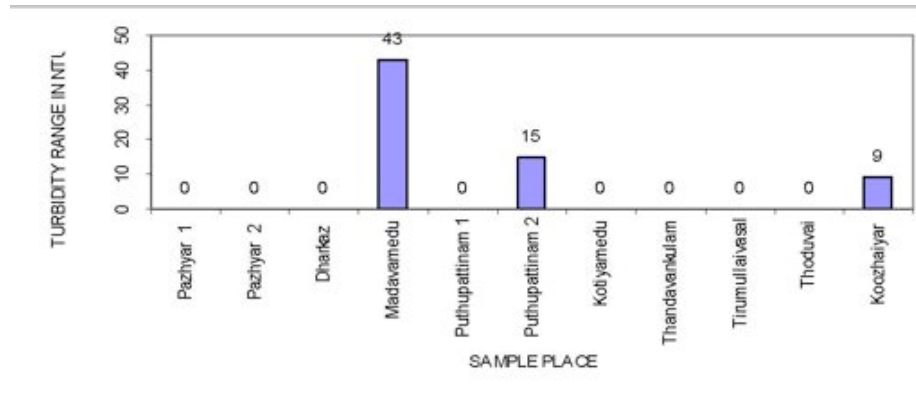


Figure. 2 (d): Water quality parameter (Turbidity)

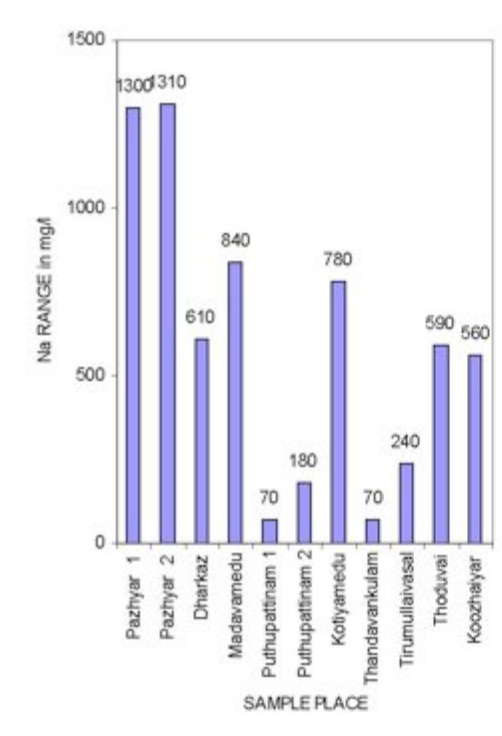


Figure. 2 (e): Water quality parameter

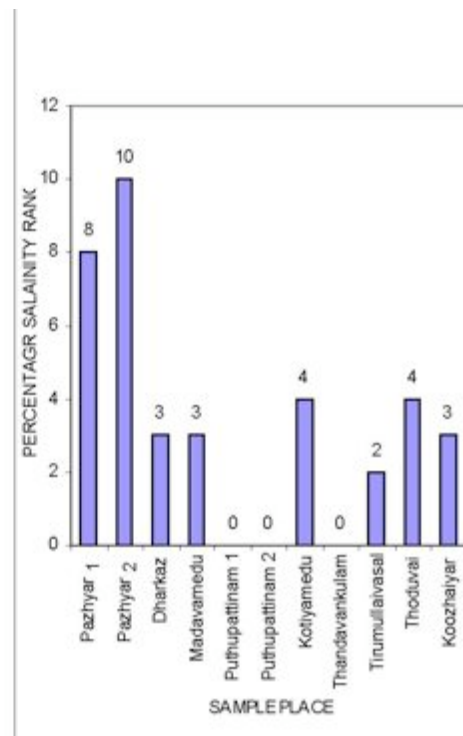


Figure. 2 (f): Water quality parameter (Na) (% Salinity)

Comparison of water samples collected from hand pumps, in general, indicated higher concentration of parameters. Water quality modeling in the study area using GIS & RS software (ILWIS) were also prepared to identify the polluted areas and these are shown in figures 3(a) and 3(b). Table 1 above and the additional figures below outline the results.

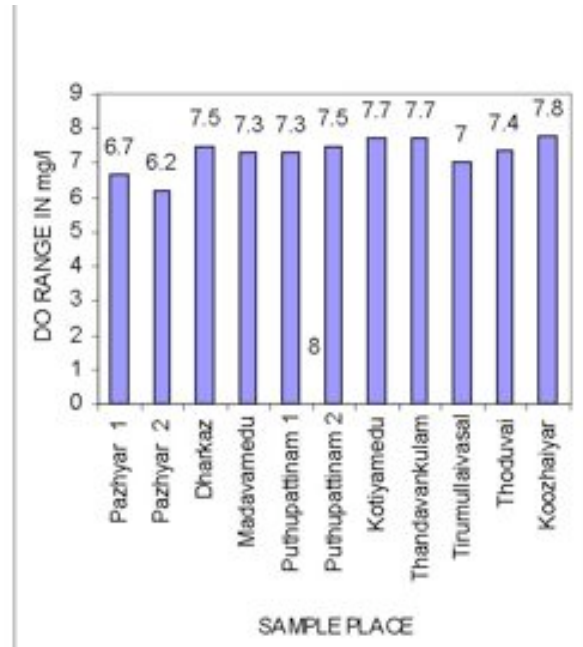
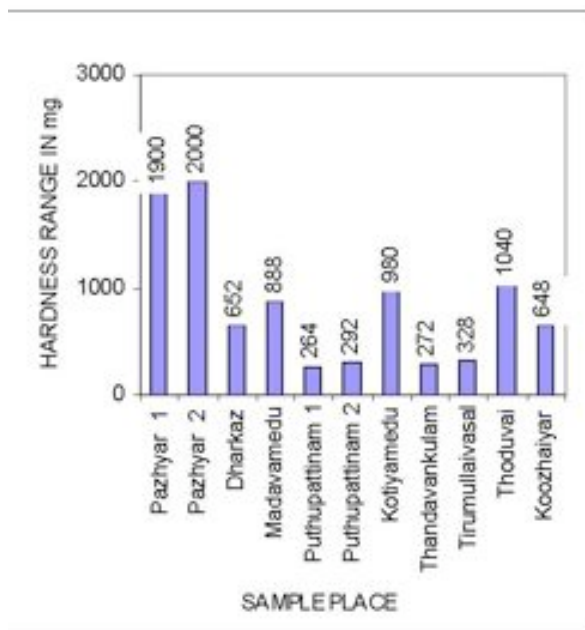


Figure. 2 (g): Water quality parameter (Hardness)

Figure. 2(h): Water quality parameter (DO)

5. CONCLUSIONS

The December 26, 2004 tsunami had a devastating effect on most of the sectors of the Tamilnadu coast, but notably in the Sirkazhi Taluck area of the Nagapatinam District. The tsunami impact changed entirely the coastal geomorphology along this region. The inland inundation of the tsunami affected the quality of groundwater. The saline intrusion contaminated and affected significantly the quality drinking water supply and affected significantly its quality parameters show very significant change due to recent Tsunami.

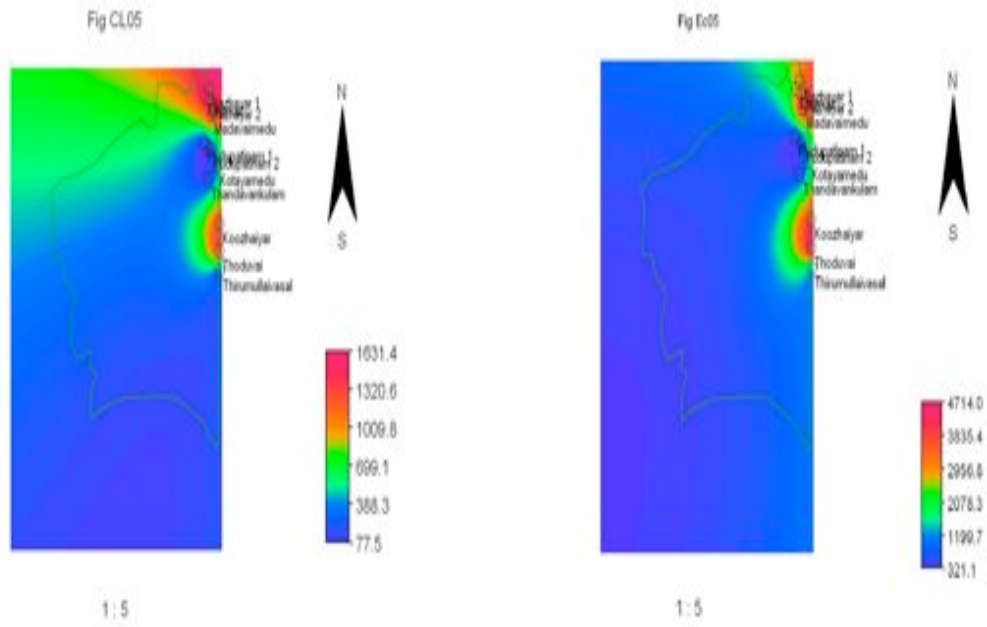


Figure. 3 (a): Water quality Modeling (Cl and EC)

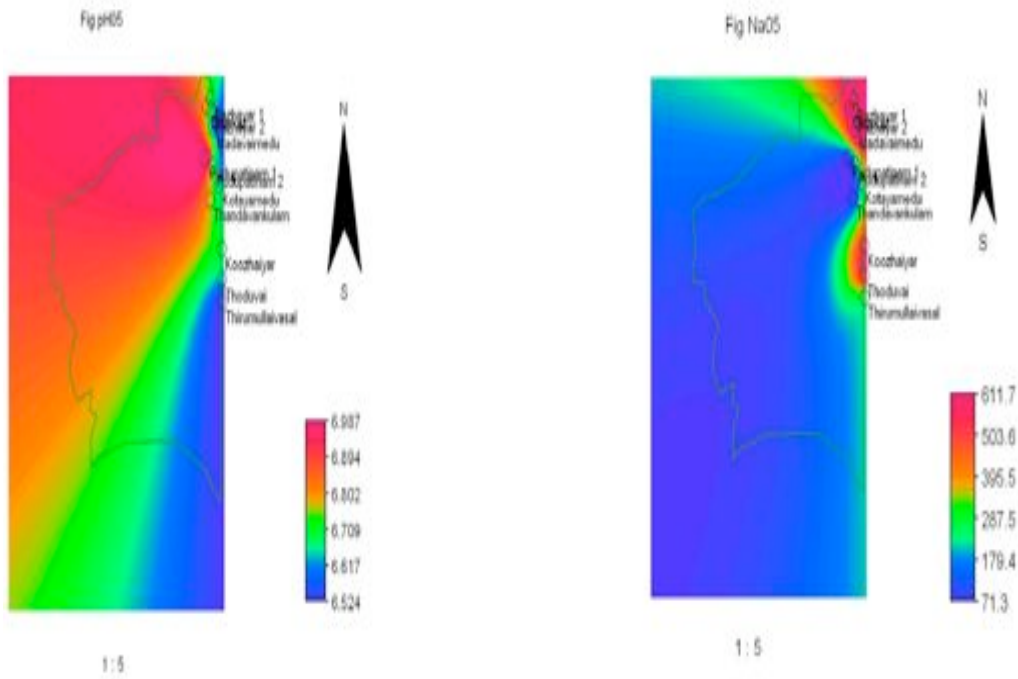


Figure. 3 (b): Water quality Modeling (pH and Na)

6. REFERENCES

- Ali, M. and T. N. Tiwari, 1998. Trace metals in the groundwater of Rourkela (India): Concentrations and correlations. *Nat. Acad. Sci. Lett.* 11(8): pp. 257-259.
- Bhargava, R. K., S. C. Saxena and V.P. Thergaonkar, 1978. Groundwater quality in Ajmer district. *Indian J. Env. Health.* 20(4): pp. 290-302.
- Gupta, S., 1981. Evaluation of the quality of well waters in Udaipur district. *Indian J. Env. Health.* 23: pp. 195-207. *Engineers India.* Vol. 1993. No4. pp. 1-14.
- M D Kudale, 2005, Interaction of Tsunami with Coastline, Indian society for Hydraulics, Proceedings of the National conference, HYDRO – 2005, pp. 83 – 91
- N P Kurian and T N Prakash, 2005, December 2004 Tsunami: An analysis of its impact on the Kerala coast, Indian society for Hydraulics, Proceedings of the National conference, HYDRO – 2005, pp. 46 - 57
- Singh, S. K., Vivek Anand, 1991. Study of groundwater quality in Jhunjhunu District (Rajasthan). *J. IPHE (I).* PP. 47-57
- Dr. S. K. Singh and P. Sunil Kumar, 1993. Physico-Chemical Characteristics of groundwater of district Karim Nagar (Andhra Pradesh). *Journal of the Institution of Public Health Engineers India.* Vol. 1993
- Ugarkar, A. G., H. M. Jayasheela. S. G. Tengainkai and S. C. Puranik, 1984. Hydro-Chemical studies of groundwater of Gadag schist belt, Karnataka. *Bull. Pure Appl. Sci.* 30(1): pp. 9-13.
- Vijay Kumar, V., D. Paul Daniel and M. Prabhakara Chary. Study of groundwater quality of Vikarabad Environs, Rangareddy District, Andhra Pradesh. *JIWWA.* Jan-Mar. 1992. PP. 123-128. World Health Organization (WHO) standards and Bureau Of Indian Standards (BIS) for drinking water quality.



Copyright © 2008
The Tsunami Society
P. O. Box 2117
Ewa Beach, HI 96706-0117, USA

WWW.TSUNAMISOCIETY.ORG